DESIGN OF A MICROFLUIDIC PLATFORM FOR REAL-TIME ENUMERATION AND RETRIEVAL OF LOW CONCENTRATION OF CELLS

A THESIS SUBMITTED TO
THE GRADUATE SCHOOL OF NATURAL AND APPLIED SCIENCES
OF
MIDDLE EAST TECHNICAL UNIVERSITY

BY

BUKET ŞAHİN

IN PARTIAL FULFILLMENT OF THE REQUIREMENTS
FOR
THE DEGREE OF MASTER OF SCIENCE
IN
BIOMEDICAL ENGINEERING

SEPTEMBER 2022

Approval of the thesis:

DESIGN OF A MICROFLUIDIC PLATFORM FOR REAL-TIME ENUMERATION AND RETRIEVAL OF LOW CONCENTRATION OF CELLS

submitted by **BUKET ŞAHİN** in partial fulfillment of the requirements for the degree of **Master of Science** i**n Biomedical Engineering, Middle East Technical University** by,

Prof. Dr. Halil Kalıpçılar
Dean, Graduate School of **Natural and Applied Sciences** _____

Prof. Dr. Vilda Purutçuoğlu
Head of the Department, **Biomedical Eng. Dept., METU** _____

Prof. Dr. Haluk Külah
Supervisor, **Electrical and Electronics Eng. Dept, METU** _____

Assoc. Prof. Dr. Ender Yıldırım
Co-Supervisor, **Mechanical Eng. Dept, METU** _____

Examining Committee Members:

Asst. Prof. Altuğ Özçelikkale
Mechanical Eng. Dept, METU _____

Prof. Dr. Haluk Külah
Electrical and Electronics Eng. Dept, METU _____

Assoc. Prof. Dr. Ender Yıldırım
Mechanical Eng. Dept, METU _____

Assoc. Prof. Dr. Barbaros Çetin
Mechanical Eng. Dept, Bilkent University _____

Assoc. Prof. Dr. Hüseyin Cumhur Tekin
Bioengineering Dept., İYTE _____

Date: 05.09.2022

I hereby declare that all information in this document has been obtained and presented in accordance with academic rules and ethical conduct. I also declare that, as required by these rules and conduct, I have fully cited and referenced all material and results that are not original to this work.

Name Last name : Buket Şahin

Signature :

ABSTRACT

DESIGN OF A MICROFLUIDIC PLATFORM FOR REAL-TIME ENUMERATION AND RETRIEVAL OF LOW CONCENTRATION OF CELLS

Şahin, Buket
Master of Science, Biomedical Engineering
Supervisor: Prof. Dr. Haluk Külah
Co-Supervisor: Assoc. Prof. Dr. Ender Yıldırım

September 2022, 88 pages

Spiking experiments are essential to characterize the performance of devices developed for rare cell recovery. However, it is challenging to spike tumor cells at very low concentrations in a standard laboratory environment with conventional methods like serial dilution, in which the variation becomes quite high. Other platforms for single-cell picking are extremely high cost and not available in standard laboratories.

We propose a low-cost, repeatable, and robust microfluidic system to spike a very low number of cells (1-100) with high accuracy, without any sample loss and dead volume. The platform included a PDMS microfluidic chip and a flexible hydraulic reservoir (FHR) connected to the outlet reservoir, providing zero dead volume. To characterize the system, fluorescently stained cells were passed through the channel and collected directly in the pipette tip connected to FHR. Cells passing through the microchannel were monitored under a microscope and counted in real-time. Then, the collected cells were transferred to a well plate and counted for comparison. The average collected cell count was 9.2±2.4, 49.4±5.9 and 98.5±6.2 for targeted 10, 50, and 100 MCF7 cells, respectively. The counting accuracy was demonstrated by

linear regression between real-time versus retrieved cell counts with an R^2 of 0.9964. The microfluidic platform does not affect cell viability.

The proposed system provides low-cost and robust technique for accurate spiking of low number of cells for analytical performance characterization of rare cell isolation platforms or any other analytical study requiring few cells.

Keywords: Microfluidics, Cell Retrieval, Cell Enumeration, Zero Dead Volume

ÖZ

DÜŞÜK KONSANTRASYONLU HÜCRELERİN GERÇEK ZAMANLI SAYIMI VE TOPLANMASI İÇİN BİR MİKRO AKIŞKAN PLATFORM TASARIMI VE KARAKTERİZASYONU

Şahin, Buket
Yüksek Lisans, Biyomedikal Mühendisliği
Tez Yöneticisi: Prof. Dr. Haluk Külah
Ortak Tez Yöneticisi: Doç. Dr. Ender Yıldırım

Eylül 2022, 88 sayfa

Nadir hücrelerin geri kazanımı için geliştirilen cihazların karakterizasyonu için spiking deneyleri önemlidir. Ancak, seri seyreltme gibi varyasyonun oldukça yüksek olduğu geleneksel yöntemlerle standart bir laboratuvar ortamında çok düşük konsantrasyonlarda tümör hücreleri toplamak zordur. Tek hücre toplamaya yönelik diğer platformlar son derece yüksek maliyetlidir ve standart laboratuvarlarda mevcut değildir.

Çok düşük sayıda hücreyi (1-100) herhangi bir numune kaybı ve ölü hacim olmadan yüksek doğrulukla toplamak için düşük maliyetli, tekrarlanabilir ve sağlam bir mikroakışkan platform öneriyoruz. Platform, bir PDMS mikroakışkan çip ve çıkış rezervuarına bağlı, sıfır ölü hacim sağlayan esnek bir hidrolik rezervuar (FHR) içerir. Sistemi karakterize etmek için, floresanla boyanmış hücreler kanaldan geçirilmiş ve doğrudan FHR'ye bağlı pipet ucunda toplanmıştır. Mikro kanaldan geçen hücreler mikroskop altında izlenmiş ve gerçek zamanlı olarak sayılmıştır. Ardından, toplanan hücreler bir kuyu plakasına ekilmiş ve karşılaştırma için sayılmıştır. Toplanan ortalama hücre sayısı hedeflenen 10, 50 ve 100 MCF7 hücresi için sırasıyla 9,2±2,4-49,4±5,9 ve 98,5±6,2 olarak bulunmuştur. Sayım doğruluğu, gerçek zamanlı ve

toplanan hücre sayıları arasındaki doğrusal regresyon (R^2=0,9964) ile gösterilmiştir. Mikroakışkan platform hücre canlılığını etkilememektedir.

Önerilen sistem, nadir hücre izolasyon platformlarının analitik performans karakterizasyonu veya az sayıda hücre gerektiren diğer analitik çalışmalarda düşük sayıda hücrenin doğru şekilde sayılması için düşük maliyetli ve sağlam bir teknik sunmaktadır.

Anahtar Kelimeler: Mikroakışkan, Hücre Toplama, Hücre Sayımı, Sıfır Ölü Hacim

To my dear family

ACKNOWLEDGMENTS

I would like to express my special thanks to my supervisor Prof. Dr. Haluk Külah for the support, encouragement, and supervision throughout my study and also for giving me the opportunity to work on an exciting project. I am also grateful to my co-advisor, Assoc. Prof. Ender Yıldırım for his valuable guidance and much-appreciated comments.

I am deeply grateful to Mikro Biyosistemler family for their support. I would like to express my gratitude to Assoc. Prof. Ebru Özgür and Dr. Özge Zorlu for their invaluable remarks, opinions, and motivations. I am grateful to Dr. Begüm Şen Doğan for sharing her knowledge and experience with me whenever I need. Also, many thanks to Taylan Töral for helping me during the fabrication of my devices. Moreover, I am particularly thankful to Gizem Karayalçın for preparing cancer cell lines for my experiments. I would like to thank to Micromanufacturing Laboratory group at METU Mechanical Engineering Department for fabrication of the brass mold and FHR. Many thanks to Alper Demir and Ege Mutlu, who gave me guidance, enthusiasm, and patience during my work. I would also thank Nilüfer Afşar Erkal, Şebnem Şahin, Emel Çiftçi and Salih Balta to create a very enjoyable environment.

This author is financially supported by Scientific and Technological Research Council of Turkey (TUBİTAK) BİDEB 2210-A graduate scholarship during this study.

Finally, I would like to, most importantly, express my deepest thankfulness to my dear mother, Kadriye Şahin, my dear father, Yüksel Şahin, and my dear sister, Burcu Şahin, for their support, care and faith throughout my whole life. Thank you for always being there for me. A debt of gratitude is also owed to Mehmet Faruk Özkan for his endless love, patience and never leaving me alone.

TABLE OF CONTENTS

LIST OF TABLES

TABLES

LIST OF FIGURES

FIGURES

CHAPTER 1

INTRODUCTION

Since the first emergence of the term microfluidic, the growing interest in the development and utilize of devices that allow the use of fluids on a micro-scale continues to increase. Microfluidic systems are systems consisting of micro-sized (10-1000 μm) channels and allow to process of very low volumes of liquids [1]. Microfluidics has become a critical enabling technology for many applications in life sciences and diagnostics [2]. This multidisciplinary technology is employed in various applications, from the development of drug delivery systems to chips utilized for diagnostic purposes, from cell manipulating structures to cell counter systems [3]. This technology is often applied to point-of-care diagnostic solutions, given that they perform operations using conventional systems at much lower volumes and more quickly.

Microfluidic devices with low sample volume requirements, fast processing times, multiplexed capabilities, and high surface-area-to-volume ratios offer an alternative for in vitro cell sorting, detection, and single-cell analysis [4]. Several microfluidic platforms are used for rare cell capture and detection based on these advantages. Thanks to these microfluidic devices, microfluidic technologies for circulating tumor cells (CTC) capture and isolation using the biological and physical properties of CTCs are still being developed and studied. CTCs are important biomarkers for cancer diagnosis and prognosis in modern medicine [5]. On average, the concentration of CTC in peripheral blood is extremely low, with as few as one to two billionths of healthy blood cells. The major challenge in isolating CTCs is that they are at very low concentrations (1-100 cells/ml) in the blood than other blood cells. Therefore, the critical factor in many CTC separation and isolation methods used is the efficiency of accurately capturing CTCs in low concentrations. It is

critical to know the cell number in characterizing the performance of any system or technology for the recovery of rare cells. Researchers perform analytical validation experiments using cell lines in a laboratory to characterize CTC isolation before using patient blood. In a process generally referred to as "spiking", researchers add a certain numbers of tumor cells into healthy blood to cover the CTC numbers in various values found in the cancer patient's blood. Thus, the system's performance in CTC isolation technologies can be characterized. CTC test specimens are traditionally prepared by diluting high concentrations of tumor cells to low concentrations by serial dilution. However, it is challenging to dilute tumor cells at extremely low concentrations in a standard laboratory environment with this method, and the variation is quite high. Although conventional cell counting technologies, such as flow cytometry are popularly used in laboratories, counting small numbers of cells with these methods is very time-consuming and impractical. To solve the problems related to accurate retrieval and spiking of low number of cells, various systems, such as cell manipulators, are used for single cell spiking and some applications, such as spiking apparatus, have been developed in the literature [6]–[12].

In this section, rare cell separation methods and cell spiking experiments will be briefly presented. Afterwards, spiking methods will be explained.

1.1 Methods for Cell Spiking

Performance validation tests are required to demonstrate the efficacy of CTC isolation methods. One of these validation studies is the determination of the recovery percentage of CTCs, which requires certain experiments to be performed under laboratory conditions before using real cancer patient blood. Researchers introduce a known amount of tumor cells into blood cells to simulate CTC isolation in these *spiking* experiments. Spiking is basically the addition of a small amount of

a known compound to a standard sample, typically to verify the performance of an analytical method [13].

In spiking experiments different amounts of cancer cell lines cultured in laboratory environments representing the CTCs are transferred into whole blood from healthy donors. Then, procedures such as red blood cell (RBC) lysis or density gradient centrifugation method is performed to get rid of RBCs. The prepared suspension containing white blood cells and spiked cancer cells is then transferred to the to the CTC separation platform, and CTC enriched sampled retrieved from the product outlet, while the rest of the sample is discarded through a waste outlet. The number of retrieved CTCs in the product is then counted by different means (e.g. fluorescent labeling and counting under microscope) and compared with the number of spiked CTCs to quantify the performance of the CTC isolation method. However, to check the accuracy of the method, it is necessary to know the exact number of spiked cells given to the isolation device and compare it with the number of cells collected at the end of the process. Therefore, cell counting methods are used to prepare the inlet sample for spiking experiments.

Cancer patients have 1-100 cells/ml of circulating tumor cells, so test samples are usually prepared within a certain range (low to high number) in the desired number to cover these clinical numbers [14]. When preparing a high concentration sample, conventional methods such as serial dilution can be used. However, when a low concentration sample is to be prepared (below 100 cells), cells must be loaded one by one into the medium, and the number must be estimated accurately. In this section, the methods developed for single cell isolation will be discussed under four main headings. These are serial dilution, flow cytometer (fluorescence-activated cell sorting), micromanipulation and microfluidic devices. Similar studies in the literature will also be exemplified.

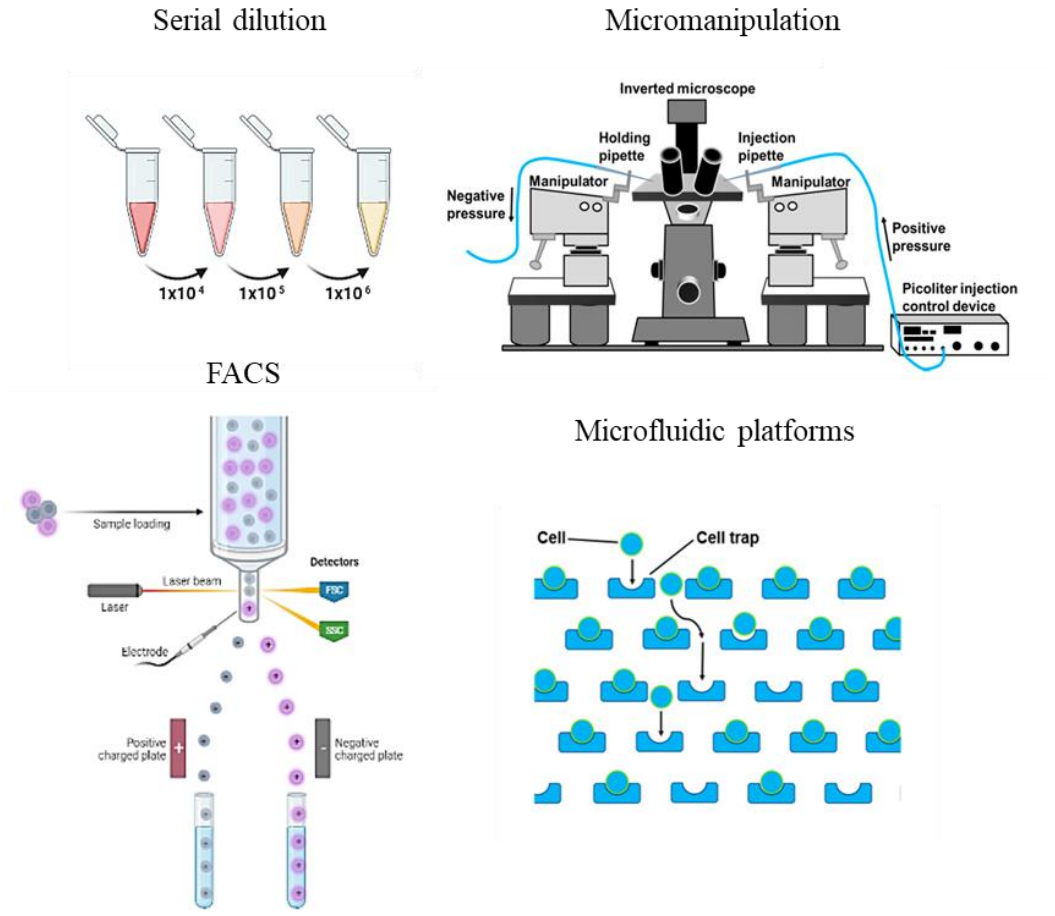

Figure 1.1 Schematic overview of low cell isolation methods [15]

Figure 1.1 illustrates the schematic of the operating principles of these four methods, which will be discussed in more details in the following. These can be classified under four headings: serial dilution, micromanipulation, flow cytometry, and microfluidic devices.

1.1.1 Serial Dilution

The simplest and the most common established method for counting cells is serial dilution [16]. Although serial dilution is simple to operate and low cost, it is prone to error and cell loss, and does not allow desired cells to be obtained [17]. The serial dilution approach is largely based on the assumption that the sampling is statistically

representative and involves gradually diluting a cell suspension with manual pipettes until a very low number of cells are obtained in individual reservoirs (Figure 1.1) [18]. When each small sample is taken, the concentration of cells in it is assumed to be the same as in the remaining solution. While this assumption is reasonable for high-concentration cells, it is susceptible to error if the operator is inconsistent in maintaining cell homogeneity in solution (for example, vortexing or pipetting) or cells are highly diluted to the point where the sample is no longer statistically representative [7]. The variation is quite high when the cell concentration is extremely low [6].

1.1.2 Flow Cytometer

Flow cytometers are the most commonly used cell counting methods with high accuracy. Furthermore, it is a technology that automatically analyzes and detects individual cell particles in the flow. In particular, patents and methods were established by Moldavan in 1934 [19], Gucker in 1947 [20], Coulter in 1953 [21], Fulwyler in 1965 [22], [23] and Dittrich and Göhde in 1968 [24] have shaped the success of commercial flow cytometry [25].

One of the most common flow cytometry methods is fluorescence-activated cell sorting (FACS), as shown in Figure 1.1. FACS systems employ fluorescence detection technologies to offer very precise cell counts with specific characteristics [26]. FACS systems use laser excitation and provide a number of analysis possibilities. This enables them to identify cell types of the same size within the same sample [27]. Cell suspensions are pressurized through a flow cell, and the sample is focused into a narrow stream with a sheath fluid that takes advantage of the hydrodynamic focusing effect. The sample flow is adjusted if the focused stream width equals the cell size, and only one cell is detected at a time [15]. Following such an arrangement, cells bound to fluorescently labeled antibodies are stimulated by laser light [28]. The fluorescent and scattering signals from each cell are then

captured by multiple optical detectors. The change in voltage value read from the detectors indicates cell passage, and so the cells may be counted based on these voltage changes. It is also possible to gather more information about cells, such as their size. Following examination, the stream is split into droplets, each of which contains a single cell. An electrical charge is delivered to the droplet depending on the fluorescence signal of the cell. Using the electrically charged plate, the charged droplet is directed into the collecting vessel for further analysis [15].

The FACS approach has the advantages of high accuracy, high sensitivity, high efficiency, and the ability to select unbiased isolation [29]. However, the entire system is bulky, complex, and expensive, and the emergence of microfluidic chip technology is expected to miniaturize the overall system. The disadvantages of this method are the requirement for a large number of suspended cells as the inlet suspension, which may influence cell groups with low abundance. Apart from that, high liquid velocity and fluorescent dye can harm cell viability. FACS experiments necessitate extensive sample preparation and a high number of cells [30]. Flow cytometer devices are a standard method when it is desired to classify highly concentrated heterogeneous populations based on their characteristics, but it is a complex, unnecessary, and expensive method when only low cell counts are targeted.

1.1.3 Manual Cell Picking/ Micromanipulator

Micromanipulation is a technique for picking individual cells using mechanical micromanipulators or optical tweezers [31]–[33]. Traditionally, the inverted microscope consists of ultra-thin glass pipettes for cell aspiration, motorized movable mechanical stage to move pipette as seen in Figure 1.1. The micropipettes are made of thin glass capillaries connected to the aspiration unit. The cell sample is supplied as a suspension in a dish or well plate. While following the process under the microscope, the operator selects a specific cell, brings the capillary tip close to the cell, and aspirates the cell by applying suction to the micropipette [15]. The

targeted cell-containing aspirated fluid is transferred to a collection vessel. This process is usually performed manually and requires the use of an inverted microscope or stereo microscope with magnification up to 200X [34].

With the availability of micromanipulators, it is now possible to take cells one at a time and drop them into a medium [7], [35]. However, the use of micromanipulators is time-consuming and expensive. The method is reasonable for injecting a small number of cells, but after a few iterations, this becomes laborious [7]. Micromanipulators allows for the controlled isolation of certain cells from a solution. Although micromanipulation enables the visual examination of single cells during separation, its inefficiency and time-consuming nature limit its widespread application. Another problem is that mechanical shearing generated by the micropipette or capillary tips might cause cell injury during manipulation [36]. Furthermore, because it demands technical expertise and precision, an untrained operator is likely to fail [29], [37]. Patented technologies established in the industry in recent years (for example, Eppendorf TransferMan® 4r, CellCelector, CytePicker®) have demonstrated great accuracy and reproducibility in obtaining correct cell numbers [38]. In addition to commercialized micromanipulators, there are also studies that have been developed for single cell transfer. For example, Müller et al. [39] developed a polyethylene cell collector and Sun et al. [40] developed a robotic micromanipulation system for cell aspiration and positioning with a micropipette.

Amontree et al. [6] designed a single-cell-spiking apparatus to replace serial dilution by producing reliable low-concentration cell samples for CTC isolation. They used a method to operate solely from capillary aspiration without the need for external laboratory equipment. The principle of operation of the device is as follows (Figure 1.2): the interface was perfectly sealed before use. The tubing's initial pressure is equivalent to atmospheric pressure. When the capillary was lowered for immersion in the sample, the capillary effect drew a little amount of liquid into the capillary tube. When a cell is targeted, the tubing is disconnected. The target tumor cell is

aspirated gently into the microcapillary tip until pressure and velocity are equal. After capturing the tumor cell, the syringe is reattached to the capillary. The trapped tumor cell is then injected into the new buffer. They validated the captured cell number with a hemocytometer. The average transfer time for SCS was 2.54 ± 0.45 minutes/cell.

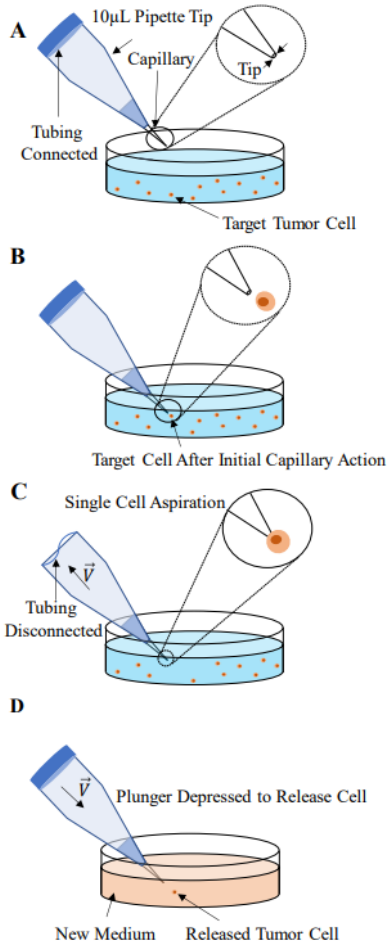

Figure 1.2 Capillary action spiking procedure a) Capillary action cell capture setup. b) The capillary tip approaches the target cell. c) The target tumor cell is aspirated into the microcapillary tip slightly. d) Picked cell is transferred to buffer [6].

Zhao et al. [7] developed a capillary-based cell-enumeration and cell-spiking apparatus (Figure 1.3). Cell suspension (4 μl) was siphoned into a glass capillary using a rubber bulb and counted manually under the microscope while in the capillary. To eject cells, the glass capillary was inserted into a disposable positive-

displacement pipet tip, and the capillary content was expelled by pushing in the piston at a constant speed. The numbers of cells ejected from a capillary were verified with an automated cytometer. The ratio between cells counted manually while in the capillary and cells counted with an automated cell cytometer after ejection was 97%.

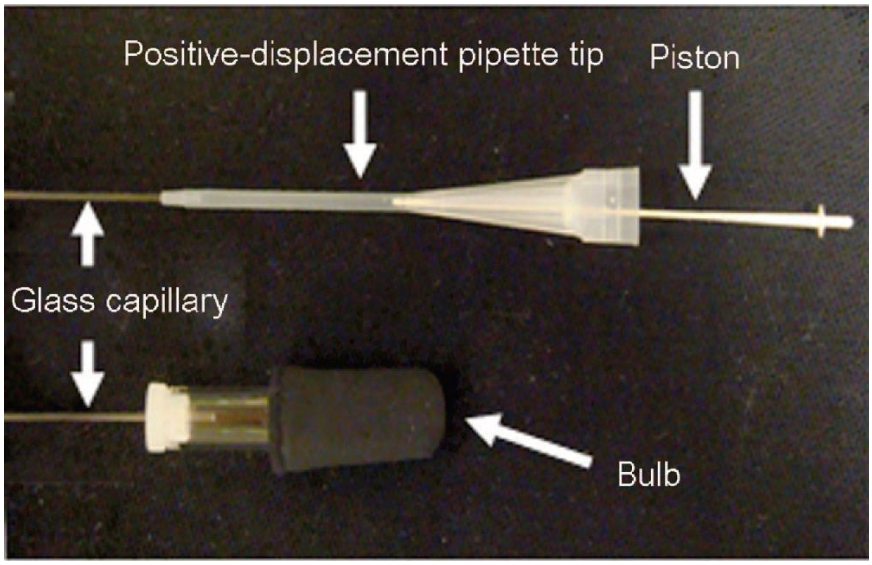

Figure 1.3 Capillary-based cell-enumeration (lower) and cell spiking (upper) devices [7]

1.1.4 Microfluidic Devices

Microfluidics is seen as a powerful technology as it provides precise fluid control, low sample consumption, device miniaturization, low cost, and easy handling of valuable fluids [41]. Microfluidic devices have been widely employed for cell isolation, enumeration, and transfer in recent years due to their minuscule size (similar to the size of a cell) and the ability to integrate numerous processes [42]. Compared to traditional methods, microfluidic technology is also economically advantageous as it can be operated in low volumes in terms of cell samples [43]. Apart from this, they can obtain accurate results with high resolution and sensitivity. Hydrodynamic cell traps and droplet techniques are two common working principles of microfluidic devices [15].

Droplet-based microfluidics uses oil-filled channels to trap aqueous droplets. Because they can hold a single cell, these droplets can also be counted one by one. The efficiency of these procedures is their main advantage [44]. Ding et al. [8] performed a single-cell capture, isolation, and retrieval method via a static droplet array (Figure 1.4). In this method, the chip is temporarily bonded to the substrate during the injection. After cells were injected into the chip at a concentration of $5x10^3$ cells/ml and an operating rate of 90 µl/min, they were captured inside the chip. Then the device is frozen, and the chip peeled off. The freezing process ensures that the droplets adhere to the substrate after the chip peel-off, and droplets can be collected with a pipette. Thus, targeted cells can be transferred to the reservoir without cell loss. The entire process takes less than 15 minutes. Cell transfer rate was found to be 80% (8 out of 10 cells) on average for 10 cells and viability was found to be 86%.

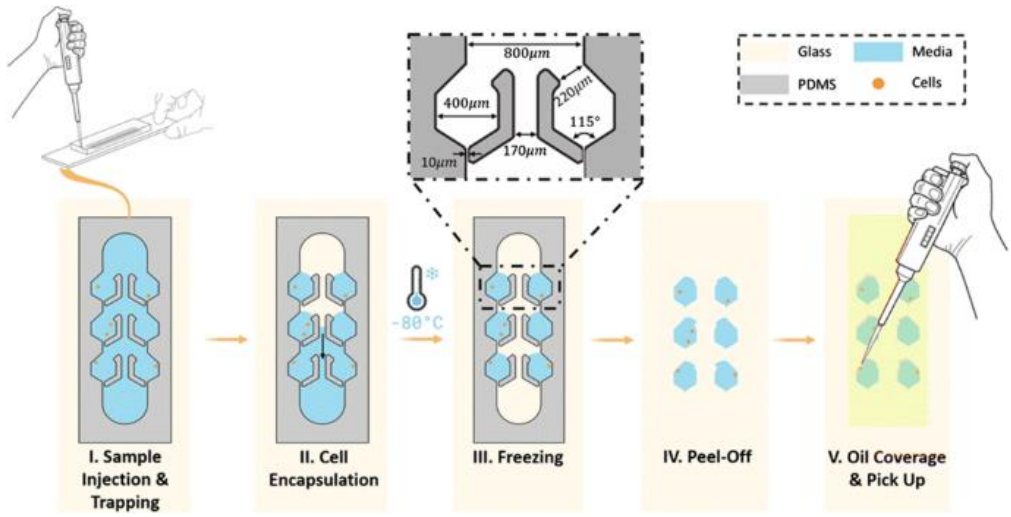

Figure 1.4 Schematic illustration of working principle of the single-cell capture and retrieve device [8]

Hydrodynamic traps allow a single cell in the microfluidic channel to enter the trap [45]. Single cells can be eliminated using this method by manually pipetting without the requirement for microscope manipulation [46]. Multiple cell trapping can be prevented by designing traps for average cell size and appropriate concentration.

However, the soft-lithography channels used in this process are prone to clogging of the cells [16]. This limits the operation of the device. For example, Hayakawa et al. [9] developed a device consisting of a cell capture unit with a microfluidic device and a cell-selective device with high aspect ratio PDMS columns (Figure 1.5).

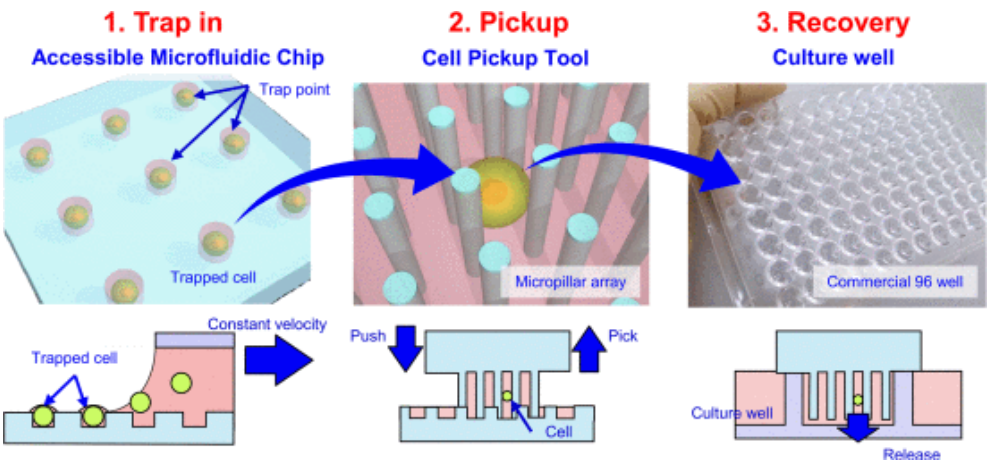

Figure 1.5 Cell separation mechanism based on accessible microfluidic chip. [9]

In this method, cells are fed into the microfluidic device first, then recovered using the cell picker tool in the system. Since the microfluidic device has an open structure, it provides easy access to the target cell. Cells trapped, one cell in each well, is opened by the PDMS pillars and recovered from the accessible microfluidic chip. After that, cells were transferred and released into culture dish. They obtained single and viable cells at 14.3% of the retrieved/targeted success rate. The captured cells show 74.5% viability.

Chen et al. [10] developed a photomechanical method to selectively isolate and retrieve target cells from closed microfluidic chambers and perform single-cell monitoring (Figure 1.6).

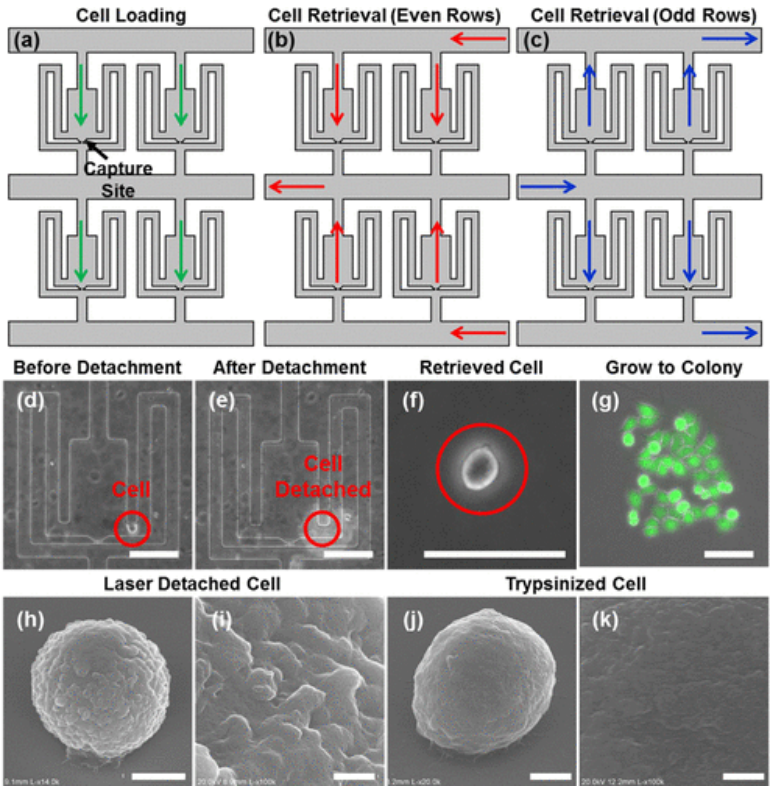

Figure 1.6 Cell retrieval process a) Cells are loaded to the channel for culturing b) cells in even rows are retrieved c) cells in odd rows are retrieved d-e) recovery process of the cells h-k) SEM images of the laser detached and trypsinized cells [10]

As shown in Figure 1.6, cells were first loaded into the microfluidic device from the inlet for culturing and captured at the capture sites as they flowed towards the outlet. Cells were fed to the chip at a concentration of $1x10^6$ cells/ml under a flow rate of 0.04 µl/min. For 24 hours, cells trapped in the chamber were allowed to stick to the substrate (cells can be cultured healthily on the chip). A focused nanosecond laser pulse was then used to separate the selected cells. Then, cells were taken from alternative parallel channels and different outlets by applying pressure from the right or left side. This device has single cell capture arrays with greater than 1000 chambers. More than 90% of the detached cells were retrieved from the outlet. The viability of the collected cells was 85.3% ± 9.6%.

Approaches to flow cytometer miniaturization using microfluidic technologies have also been developed [47]. One of the goals of this research is to bring the benefits of flow cytometers, such as cell sorting and counting, to compact, relatively low-cost, and possibly portable devices. For example, Balsam et al. [48] developed a flow cytometer based on a webcam capable of detecting low and single cell counts in a large volume (Figure 1.7). The flow cytometer was performed with a combination of a webcam, laser module for area excitation, and flow cell, providing high sample throughput over a wide flow area. Flow cytometry was able to detect and retrieve fluorescently labeled cells as low as 1 cell. To determine the counting efficiency of this platform, the number of cells counted manually with a microscope was compared with the expected number of cells. At the targeted cell counts of 100, 10, and 1, the mean cell counts measured by flow cytometry were 84, 7.9, and 0.56 cells.

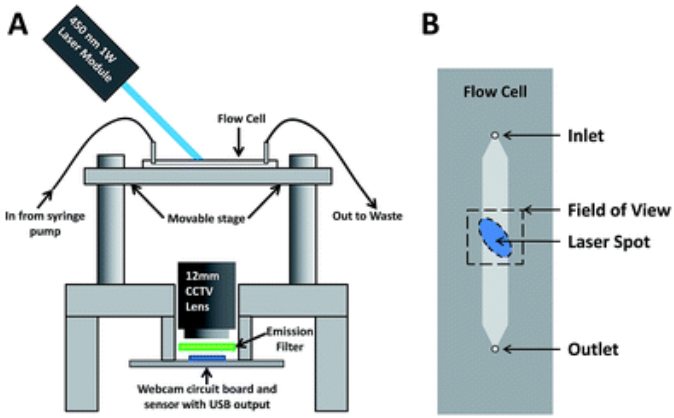

Figure 1.7 a) Schematic illustration of webcam-based flow cytometer b) Close-up view with key elements

In studies with other microfluidic methods, Yusof et al. [49], [50] reported a single-cell isolation system called a single-cell printer based on inkjet-like printing (Figure 1.8). The cell suspension is placed in the microfluidic dispersion chip fitted within a polymer cartridge. Before dispensing, the automated object identification algorithm recognizes cells in the dispenser nozzle. The cells are sorted at the chip's nozzle and then ejected in a microdroplet to be deposited on various substrates. In addition, there are investigations in the literature that combines microfluidic technology and manual

cell picker apparatus [51], [52]. A single-cell aspirator was developed by Tokar et al. After identifying the target cells in the microwells, they are aspirated into the glass pipette tip. For targeting 50 cells, 85-95% transfer efficiency was achieved which is the number collected cells versus the targeted cells [52].

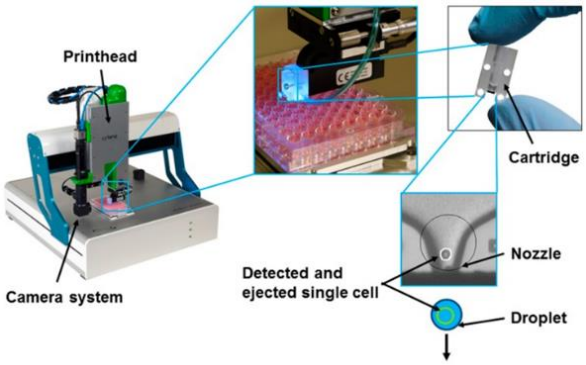

Figure 1.8 Single-cell printer device [49]

Many methods have been reported in the literature [15], [31]. Each technology developed has its own advantages and disadvantages. Table 1.1 summarizes a comparison of commonly used cell isolation methods.

Table 1.1 Overview of low cell isolation technologies [37]

Method	**Level of automation**	**Main advantages**	**Main disadvantages**	**Complexity**	**Cost**
Serial dilution	Manual	Simple operation and low cost	Counting error and cell loss	Low	$
Manual Cell Picking/ Micromanipulator	Manual	Visualization operation	Mechanical damage	High	$$$
Fluorescence activated cell sorting	Automatic	High accuracy, high sensitivity, high throughput	Large amount of material, high skill needed, considerable cost for equipment	High	$$$
Microfluidic Devices	Automatic	Flexible channel and sealing space, low sample consumption	Cell adhesion and clogging, expensive consumables	Intermediate	$$

1.2 Research Objectives and Thesis Organization

With advances in CTC isolation methods, the critical factor in evaluating the performance of the devices is the efficiency of accurately isolating CTCs in low numbers. Accurately prepared standards for cell counting are crucial to characterize the performance of any system used to recover rare cells. The preparation of these samples requires the transfer of cultured CTCs in specific numbers, one by one, into blood samples to simulate tumor cells that are rarely found in human blood. In a standard laboratory setting, it is difficult to spike tumor cells at very low concentrations by conventional methods such as serial dilution, where variation is quite high. Other platforms for single cell picking or flow cytometry are extremely costly and not available in standard laboratories.

The main research objective of this thesis is to develop a low-cost and simple microfluidic system for retrieval of very low number of cells (1-100) with high accuracy and cell viability, and without any sample loss.

To achieve this objective, the following studies are carried out in a systematic manner:

- Design and implementation of the microfluidic cell retrieval system
- Flow characterization tests
- Performance validation of the device with microbeads and MCF7 cancer cell line
- Evaluation of the proposed cell counting algorithm

In the following chapter (Chapter 2), operating principles of proposed microfluidic system is explained. In addition, the underlying theory is presented. Chapter 3 includes device design, fabrication, experimental setup, and experimental analysis. Chapter 4 presents the performance evaluation of the devices with microbeads and cancer cell lines. Chapter 5, the final chapter, summarizes the overall work and presents an outlook for future work.

CHAPTER 2

THEORETICAL BACKGROUND

This chapter includes the general background of the design parameters of the device and the underlying theory. Section 2.1 introduces the general concept including the working principle of the proposed microfluidic device. Sections 2.2, 2.3 and 2.4 present the theoretical background used in determining the design parameters. Section 2.5 provides basic information on low volume handling. Finally, Section 2.6 briefly overviews background information for the proposed cell counting algorithm.

2.1 Operation Principle of the Device

The working principle of the proposed concept to achieve the main objective is summarized as follows (Figure 2.1). Spiking the desired number of cells into the blood consists of a total of 5 steps. In step 1, fluorescently stained cells are prepared in PBS buffer and placed in the reservoir of the device for processing in the chip. In step 2, sample containing cells pass through the channel by operating the flexible hydraulic reservoir (FHR) [53] - connected syringe pump in vacuum mode for retrieval, and they are collected directly in the pipette tip connected to the FHR at the outlet. The number of cells passing through the microchannel is counted visually or by image processing. In step 3, when the targeted number of cells is achieved, cell retrieval process is completed. There is a desired number of cells on the pipette tip. In step 4, sample containing rare cells is transferred to the reservoir for cell release. In step 5, which is the final step, a buffer with a known number of cells is spiked to blood sample and then ready to use for target analysis or experiments.

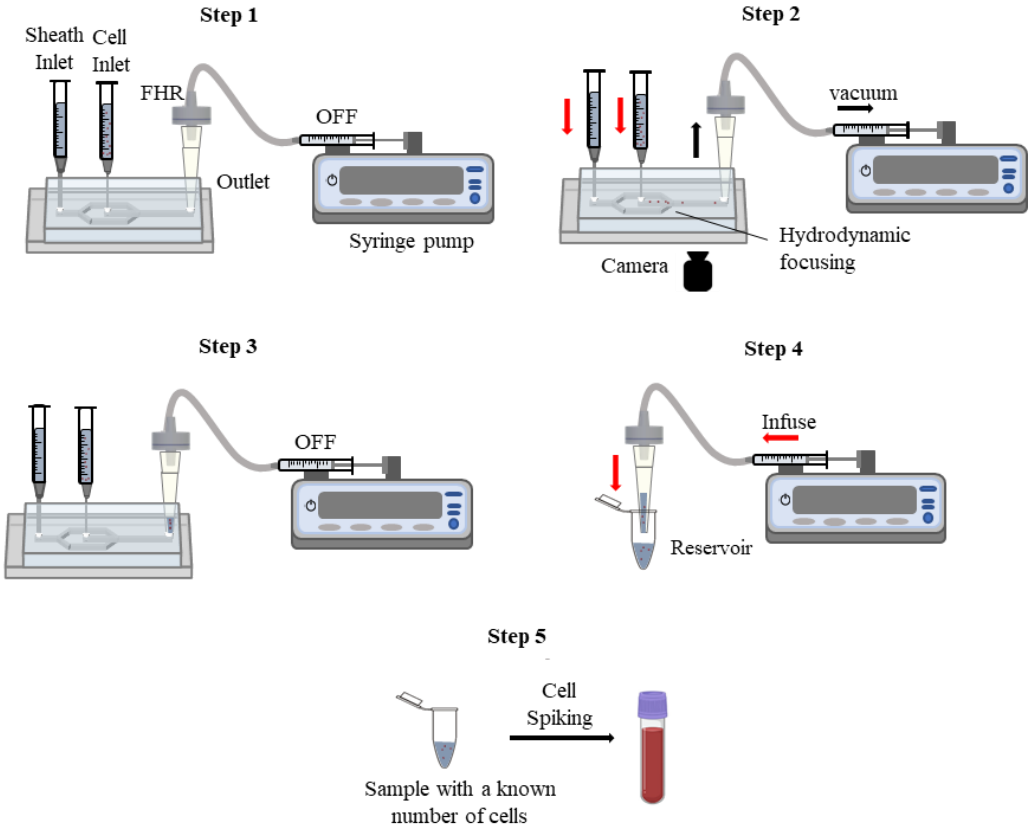

Figure 2.1 Operational flow of proposed microfluidic device

The following two main properties should be noted to design the proposed method: count cells passing through the channel in real-time and collect counted cells directly in a reservoir with zero dead volume. A channel design with hydrodynamic focusing was decided in order to count the cells in real-time with the highest accuracy. Thus, one-by-one cell passage through the observation area is ensured with the sheath flow focusing. To collect the sample containing cells passing through the channel, on-chip reservoir mechanism should be utilized. It was decided to use the FHR system in the outlet port for retrieval the sample. Theoretical knowledge to design this device is explained in the following sections.

2.2 Fundamentals of Microfluidics

Microfluidics is a field of study that investigates the behavior of fluids in small spaces. Due to the scaling of dimensions to achieve micro integration, it is necessary to study the forces and their effects at the micro-scale. Particles in fluid and suspension behave very differently at the micro-scale than at the macro-scale. Even at higher velocities, inertial forces are negligible compared to viscous forces due to the small size of microfluidics. Forces and their effects at the microscale must therefore be investigated when working with microfluidics and understanding the physics behind them is crucial. The two main types of fluids covered in microsystems are compressible fluids and incompressible fluids [54]. This study considers incompressible steady-state flow in microchannels.

The Navier-Stokes equations explains the motion of fluids (Equation 2.1). A fluid is characterized by being a continuum under the influence of external forces—that is, it is not made of discrete 'lumps'. The equation provided is for laminar flow of an incompressible Newtonian fluid.

$$\rho\left[\frac{\partial\vec{u}}{\partial t}+(\vec{u}.\nabla)\,\vec{u}\right]=-\nabla P+\rho\vec{F}+\mu\nabla^2\vec{u} \tag{2.1}$$

The left-hand side of Equation 2.1 represents the inertial forces, where the terms appearing in the parentheses represent the acceleration. Here the first term in the parentheses is the change of velocity over time, and the second term is related to the convection. The right-hand side of the equation represent the forces on the fluid, while the first term is related to the force caused by the pressure gradient, the second is related to the external body forces and the third is related to the stresses on the differential volume of fluid. The variables in the equation ρ, t, u, P, μ and F represent the density of the fluid, time, velocity, pressure in the system, viscosity, and body force, respectively [55], [56].

The above equation can be simplified for Newtonian and incompressible fluids. Hagen-Poiseuille flow is the solution of Navier-Stokes equations for steady state fully developed flow in a pipe/channel. Therefore, the part on the left side of the equation, the acceleration with respect to time, is equal to zero. Most microfluidic systems have pressure or flow source to create fluid flow. The pressure will not equal zero if a pressure gradient is created in the Poiseuille flow. The flow is steady state, the surface forces are negligible and unidirectional. Thus, the Navier-Stokes equation can be defined as in Equation 2.2 for pipe or rectangular cross-section fluid channels [55].

$$\nabla P = \mu \nabla^2 u \tag{2.2}$$

Several physical phenomena interact and act together in microfluidic systems: Reynolds number, fluid resistance, and velocity ratio are crucial factors to consider while designing a microfluidic channel. These concepts will be discussed in the following section.

2.2.1 Flow Regime

2.2.1.1 Reynolds Number

The behavior of flow in a channel is identified by the Reynolds number (Re), which is the ratio between inertial forces to viscous forces. In mathematical terms,

$$Re = \frac{\rho u D_H}{\mu} = \frac{u D_H}{\nu} \tag{2.3}$$

where ρ is the density of the fluid, u is the velocity of the fluid flow, D_H is the hydraulic diameter of the channel, μ is the dynamic viscosity of the fluid, and ν is the kinematic viscosity of the fluid, respectively [57]. The hydraulic diameter is considered the diameter of the circular tube. However, because in microfluidics

channels are often rectangular cross sections, the hydraulic diameter for a non-circular cross-section is calculated as follows

$$D_H = \frac{2wh}{(h+w)} \tag{2.4}$$

where w and h are the width and height of the channel, respectively.

Due to micro scale of the characteristic dimension of the flow, Reynolds number is very low in microfluidic devices and the flow is laminar (1< Re <2300). In laminar flow, the velocity of a particle in a fluid is not an arbitrary function of time. Liquid particles do not mix in laminar flow and travel along the smooth path of the layers. Low Reynolds numbers also imply that viscous forces dominate inertia forces at the microscale. Viscous forces occur when fluid slow down as a result of friction, such as around a channel wall [58]. When the Reynolds number is much smaller than 1, laminar flow in microfluidics can be classified as Stokes flow regime, where fluid velocities are very low, viscous effects are very large and flow can be shown with Stokes Law [59].

Laminar flow is a condition when the velocity of the particle in a flow doesn't change randomly over time. Because of laminar flow, two or more flows that come into contact with each other don't mix unless they move through each other.

2.3 Theoretical Calculation of Symmetric Hydrodynamic Focusing

When designing a 2D focusing channel on a microfluidic device, some aspects should be considered. In hydrodynamic focusing, the width of the flow is narrowed by introducing a sheath flow around the main flow that is carrying suspended cells. The cells are pinched in the middle of the channel. This makes it easier to predict cells' position and stable the velocity [60]. To get precise features in cell counting, the width of the focused stream should be in the order of the cell size.

This section describes existing theoretical models for two-dimensional hydrodynamic focusing in rectangular microchannels (Figure 2.2). In the described theory and in this thesis, the following conditions are assumed: the working fluids are Newtonian and have the same density (ρ) and viscosity (μ). Also, inlet, outlet and side channels have the same height (h). In the studied geometry and flow conditions, the Reynolds number Re is less than 1 depending on the fluid velocity, so the flow is steady and laminar [61].

As shown in the Figure 2.2 the sample enters from the inlet channel with a flow rate Q_i and calculated as $Q_i = v_i\, w_i\, h$, where average inlet flow velocity is v_i, width is w_i and height is h, respectively. Sheath flow applied from the side channels, with a volumetric flow rate of Q_s and width of w_s. Q_o is the final flow rate at the outlet channel ($Q_o = v_o\, w_o\, h$). In this study, 2-D symmetric hydrodynamic focusing is used, where the sheath flow rates from the side channels are the same.

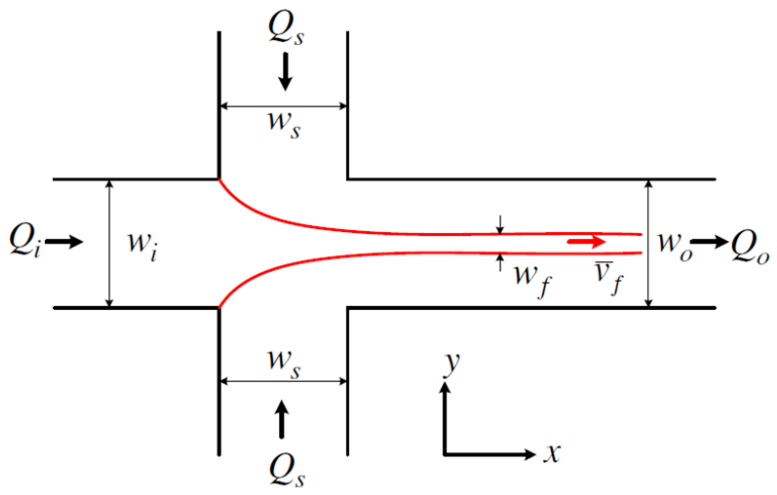

Figure 2.2 Schematic of the 2D symmetric hydrodynamic focusing in the rectangular microchannel. Q_i, Q_s and Q_o are the volumetric flow rate at the inlet, sheath, and outlet, respectively [61]

The principle of mass conservation states that the amount of sample entering to inlet channel is the same as the amount of sample passing through the size of the narrowed focused stream.

$$v_f\, w_f\, h = Q_i \tag{2.5}$$

where v_f is average flow velocities of the focused stream, w_f is focused stream width, h is height of the channel and Q_i is inlet channel a flow rate. In addition, the total amount of liquid at the outlet channel is the same as the sum of the amount of liquid delivered through the inlet and side channels, mathematically,

$$Q_o = Q_i + 2Q_s \tag{2.6}$$

The following equation is obtained to determine the relationship of the focused stream width (w_f) with other parameters.

$$\frac{w_f}{w_o} = \frac{Q_i\, h}{\frac{v_f}{v_o} Q_o\, h} = \frac{Q_i}{\frac{v_f}{v_o}(Q_i + 2Q_s)} \tag{2.7}$$

where Q_i and Q_s are the volumetric flow rates of inlet and side channels, v_f and v_o are the average flow velocities of the focused stream and outlet channel, h is the height of the channel, respectively. v_f/v_o ratio is the only unknown parameters in the equation to estimate the focused flow width. Since Reynolds number is low, flow is in laminar regime, flow is incompressible and fluid is Newtonian. Therefore, the Navier-Stokes equation is used. The velocity is axial and varies with lateral coordinates $u = u(y, z)$. This means the flow is fully developed. If the Navier-stokes equation is solved according to the no-slip condition on the channel wall, the solution is as follows [62];

$$u(y,z) = \frac{4h^2}{\mu\pi^3}\left(-\frac{dp}{dx}\right)\sum_{n=0}^{\infty}(-1)^n \left\{1 - \frac{cosh[(2n+1)\pi y/h]}{cosh[(2n+1)\pi w_o/2h]}\right\}\frac{cos[(2n+1)\pi z/h]}{(2n+1)^3} \tag{2.8}$$

Where u is streamwise average velocity, μ is dynamic viscosity, $-w_o/2 \leq y \leq w_o/2$ and $-h/2 \leq z \leq h/2$, the h is the height of the channel. Equation 2.8 describes the Poiseuille velocity profile for rectangular microchannels [62]. If the

equation is integrated with the boundary condition along the z direction, average flow velocity is obtained. Using this equation, the velocity in the outlet channel and the velocity of the focused flow can be obtained [63]. Afterward, outlet channel average velocity and focused stream average velocities can be determined using the Equation 2.8. The ratio of the average flow velocities is expressed as follows.

$$\frac{v_f}{v_o} = \frac{\left\{1 - (192h/\pi^5 w_f) \sum_{n=0}^{\infty} \frac{1}{(2n+1)^5} \frac{sinh[(2n+1)\pi w_f/2h]}{cosh[(2n+1)\pi w_o/2h]}\right\}}{\left\{1 - (192h\ /\ \pi^5 w_o) \sum_{n=0}^{\infty} \frac{tanh[(2n+1)\pi w_o/2h]}{(2n+1)^5}\right\}} \quad (2.9)$$

According to Equation 2.9, the volume ratios depend on the focused flow width, outlet channel width and channel height.

2.4 Hydrodynamic Resistance and Capacitance

The flow of a liquid can be thought of as the flow of electricity; liquid molecules in a hydraulic circuit behave like electrons in an electrical circuit. This well-known hydraulic circuit analogy may be directly used to estimate the flow/pressure relationship based on basic electrical circuit theory. The formulas and relationships between voltage, current, and resistance are physically similar to those between pressure, flow rate, hydraulic resistance [64].

In microfluidics, a pump or syringe creates a pressure increase at the inlet. The fluid drives through the channel with created pressure drop. This pressure difference can be described by the fluid analogous Ohm's law ($\Delta V = RI$, I is electrical current, R is electrical resistance, ΔV is electrical potential difference) [65]:

$$\Delta P = RQ \quad (2.10)$$

where ΔP is the pressure difference across the channel, Q is the flow rate and R is the fluidic resistance. For cylindrical tubing, hydraulic resistance is defined as,

$$R_H = \frac{8\mu L}{\pi r^4} \tag{2.11}$$

where μ is dynamic viscosity of fluid, L is length of the tubing, r is the inner radius of the tubing, respectively. For rectangular microchannel with $w > h$, the hydrodynamic resistance is calculated as [66]:

$$R_H = \frac{12\mu L}{wh^3\left(1 - \frac{0.63h}{w}\right)} \tag{2.12}$$

where, L is channel length, w and h are the width and height, respectively. Since the liquids and channels are not completely rigid, a pressure change occurs. This causes a change in the volume of the fluid. Explained situation is similar to capacitance in an electrical circuit.

There is hydraulic compliance effect of microchannels and tubing. In addition, due to the air trapped in the microchannel, air capacitance occurs. The compliance of the gas is very large compared to the liquid and the channel wall, so the last two are negligible [65]. The air capacitance (C_a) is calculated by the following formula:

$$C_a = \frac{V(t)}{P} \tag{2.13}$$

where the P is internal pressure, V is the instantaneous volume.

2.5 Low Volume and Zero Dead Volume Handling

Since the fluids used in microfluidic systems can carry valuable particles or cells, the sample losses may be critical. These losses occur during the fluid loading and transfer steps. Syringe pumps or pressure control devices are generally used to generate fluid flow in microfluidic systems [67]. When syringe pumps are used,

considerable dead volume is seen due to the air bubbles or Luer mechanism at the tip of the syringe. Similarly, in pressure control devices, there is a very large dead volume in the connection parts. Since the main purpose of this thesis is to retrieve low number of cells with minimum loss and low volume, sample loading interface called the flexible hydraulic reservoir developed by Hatipoğlu et al. [68] was used. This design has been developed to transmit valuable liquids at the desired flow rate and volume to the microfluidic channels. It is based on Pascal's principle. According to this principle, when pressure is applied to a liquid in a closed container, the pressure is transmitted equally in all directions [68]. When hydraulic pressure is created by a pump, the same force applies on all parts of the membrane regardless of position. Hydraulic pressure can be explained as the pressure exerted by a fluid that delivers the force in all directions. Thus, the pressure generated by the pump can be completely transmitted through the membrane.

The flexible hydraulic reservoir mechanism basically consists of three elements hydraulic and sample chamber and a nitrile membrane in the middle separating these two chambers (Figure 2.3 part (b)). The hydraulic chamber is filled with dummy fluid, the sample chamber is empty in the default position. An incompressible fluid must be used in the interconnection tubing from the syringe pump to the top chamber and in the hydraulic chamber. There is a reservoir connected to the sample chamber of the FHR. This reservoir part is directly connected to the microfluidic device and collect the valuable liquid which is regulated by the FHR-connected syringe pump with zero dead volume.

The working principle of the system is as follows (Figure 2.3): first, the tubing, which is the interconnection element, and the upper chamber of the FHR are filled with liquid. When the incompressible hydraulic fluid is pumped into the hydraulic chamber by the syringe pump, the force is transferred through the fluid and creates a pressure that deflects the membrane. The pressure on the membrane acts as a transmitter between the sample and the microfluidic chip. When the negative pressure is actuated, the membrane deflects toward hydraulic part, causing air to be

trapped as the sample is collected at the pipette tip. The membrane deflects as much as the volume of collected liquid. This trapped air creates a capacitive effect. However, it creates a damping effect for the oscillations generated by the syringe pump. When the positive pressure is activated, the membrane returns back to its original state, causing the sample collected at the pipette tip to be release due to the hydraulic pressure on the membrane [53].

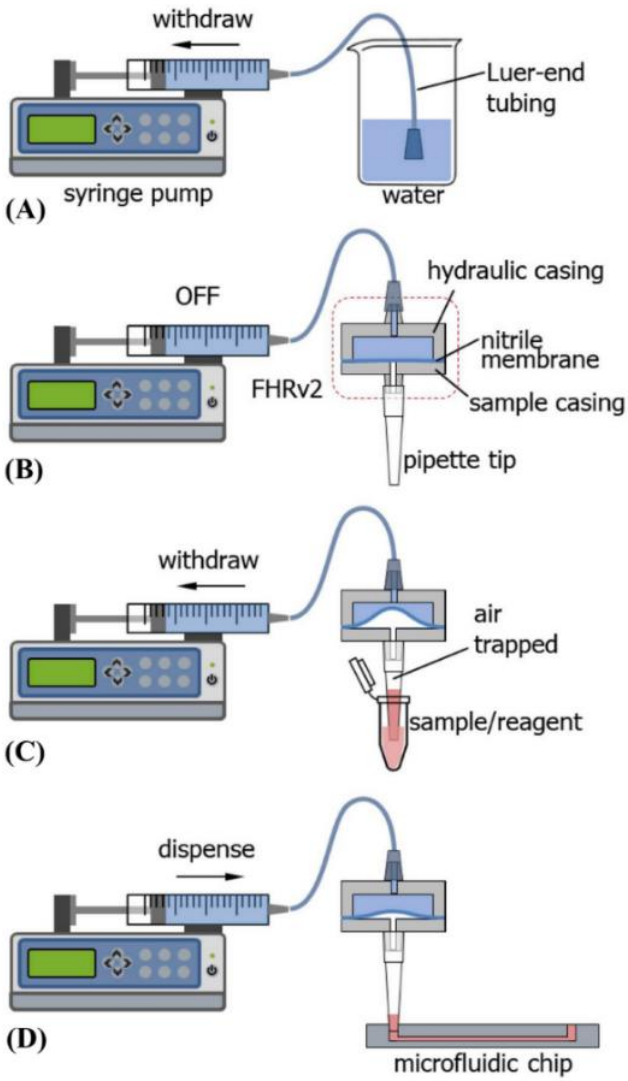

Figure 2.3 Working principle of FHR [53]

2.6 Theoretical Background of Image Processing

Image processing is a technique for performing operations on an image, such as enhancing or extracting useful information. Objects must be detected in most circumstances, which means they must stand out from the background. Various strategies have been developed for this aim, depending on the situation and the surroundings. Commonly used methods in object detection are briefly reported in this section.

2.6.1 Image Filtering

Filtering is a well-known noise reduction and image enhancement method. Although the primary function of these filters is noise reduction, they may also be used to remove certain features in an image. There are numerous ways to eliminate noise from an image, which are briefly detailed in the following section.

2.6.1.1 Mean Filter

The mean filter is a simple and easy-to-implement method of smoothing images. Each pixel value is replaced by the average value generated by neighboring pixels and itself. This eliminates pixel values that are not representative of their surroundings [69]. The size of the region to be averaged is important and has a significant effect on blurring [70]. Because each pixel has the same weight, the mean filter is easier to implement and takes less time to compute than other approaches.

2.6.1.2 Median Filter

The median filter is typically used to minimize the noise in an image, like the mean filter. However, it provides significantly better results than the mean filter in terms of preserving image details. It is commonly used since it keeps the edges while

eliminating noise. It is particularly effective at removing salt and pepper noise [70], [71].

Similar to mean filter, the median filter looks at its nearby neighbors to calculate the value of each pixel. Instead of replacing the pixel value with the average of the nearby pixel values, the median filter sorts the neighboring pixels and takes the value in the middle of the row. If the region under consideration has an even number of pixels, the median value is calculated by taking average of the two middle pixels. The sorting at each stage complicates the implementation of the median filter, especially for bigger filter sizes, which causes a high computational cost.

2.6.1.3 Gaussian Filter

The Gaussian smoothing operator is a 2-dimensional convolution operator used to 'blur' images and removes detail and noise. The Gaussian filter is a non-linear, non-uniform low-pass filter. The Gaussian filter smooths images more effectively than median filter and is primarily employed in the human visual perception system. Despite the fact that the pixels have different weights, the filter has symmetrical coefficients that make it simple to apply [70].

2.6.2 Image Segmentation

Image segmentation is the most essential stage of image analysis. Whether the analysis will be successful or not depends directly on the success of the segmentation. The process of separating an image into its parts or objects is called image segmentation. In other words, image segmentation is the process of extracting areas with the same characteristics in a homogeneous cluster, separating them from the background [72]. There are different segmentation techniques for different situations and these methods can be classified as follows.

Region Based: A region is defined as a collection of connected pixels with similar properties. This approach works well with noisy images. Region-based segmentation approaches are preferable over edge-based segmentation methods in the case of a noisy image.

Edge Based: Edges are realized by analyzing discontinuities in pixel intensities. Edge-based segmentation is based on the edges found in an image to find objects using various edge detection operators.

Thresholding: The threshold method is a simple, fast and powerful technique for image segmentation. The separation of objects from the background is done by choosing a threshold value. If pixel intensities are greater than the threshold, a pixel is segmented as an object. The simplest thresholding technique is binary thresholding. If the pixel value is less than the threshold value, it will be 0 (black). If it is larger, it will be 255 (white) [73]. Thus, this method can be used to eliminate noise below the threshold value.

CHAPTER 3

MATERIALS AND METHODS

The materials and methods section presents the microfluidic device design, device fabrication, experimental setup, and the development of a cell counter algorithm. First, the design parameters, and the fabrication of the microfluidic device are given in detail. Then, the development of the experimental protocol and the installation of the test setup are explained. Finally, the algorithm used for cell counting is reported.

3.1 Microfluidic Device Design

After determining the design parameters in Section 2.1, the design process of the microfluidic device is reported in this section. Structural features, namely the number of ports and the number of channels, and then the geometric design parameters, namely the channel depth, width, and length, were decided in a systematic manner.

Since sheath flow is used, the chip has two inlets and one outlet. Normally, when sheath flow is applied in similar systems, different syringe pumps or pressure sources are used, which complicates the operation. However, when FHR system is used at the outlet port, one single syringe pump is used as the system works in vacuum mode, which simplifies the operation. In addition, it prevents some problems, such as the difficulty of simultaneously controlling of different syringe pumps. Figure 3.1 illustrates the physical structure of the proposed chip. There are three channels in total on the chip: sheath channel, cell channel, and outlet channel.

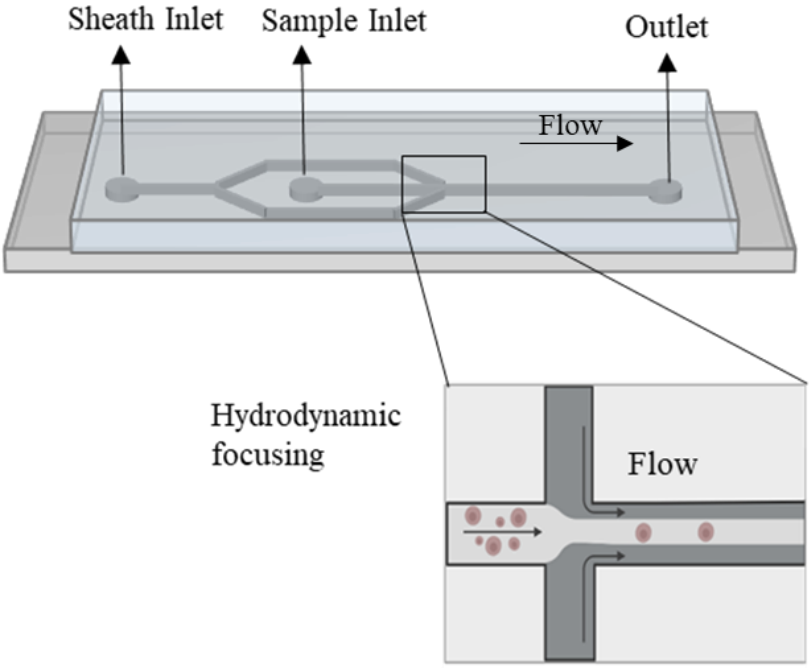

Figure 3.1 The illustration of microfluidic chip with an enlarged view of hydrodynamic focusing section

The channel depth (h) was chosen as 100 µm to avoid any clogging problems and due to fabrication limits. Average cell size of the modelled cell line is 14 µm. The width of the focused stream should be the same size as the cell size so that particles pass the focused stream one by one for accurate counting. Channel widths were chosen with a mathematical model created in MATLAB since hydrodynamic focusing, numerical solutions, coupling the hydraulic resistances should be utilized.

By substituting Equation 2.9 into Equation 2.7 in Chapter 2, the width of the focused flow can be estimated according to theoretical model developed by Lee et al. [61]. Equations are solved analytically using MATLAB. The theoretical relationship between the normalized focused flow width (w_f/w_o), and the ratio of side and inlet channel volumetric flow rates (Q_s/Q_i) is presented in Figure 3.2 for various channel aspect ratios (h/w_o).

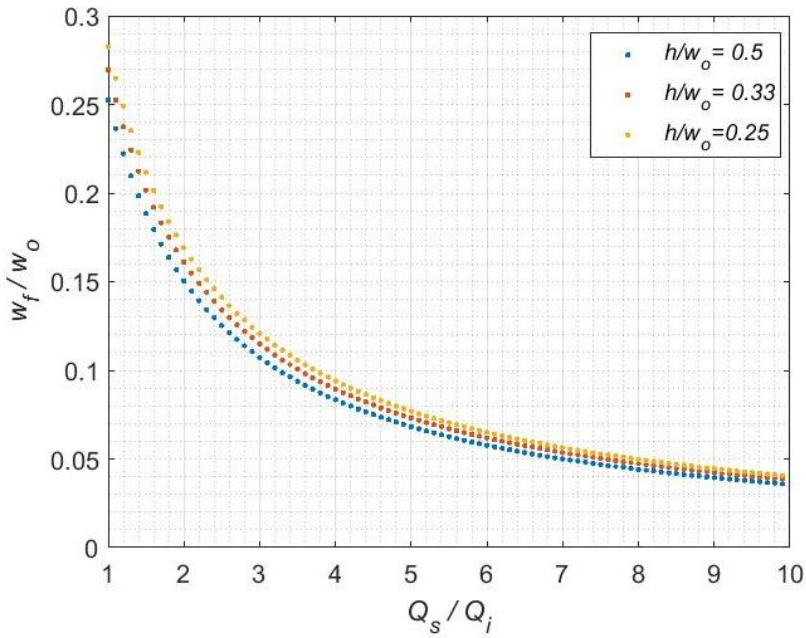

Figure 3.2 Comparison of the normalized width of hydrodynamically focused flow as a function of relative side and inlet channel flow velocity in microchannels with different aspect ratios. The graph was obtained by analytically solving the equations in MATLAB.

The following inferences can be made according to the graph. The effect of aspect ratio on velocity ratio is not significant. The volumetric flow rate ratio and the focused flow width are mutually dependent and show a nonlinear relationship. The width of the focused flow is independent of the applied flow rate but depends on the ratio of the inlet and side channel flow rates. As the flow rate ratio increases, the width of the focused flow decreases, but this change is not significant at higher rates.

In normal situations, when the inlet pressures are provided separately, the focused flow width can be easily controlled by tuning the flow rates of the sample and sheath inlets. In such cases, the width of the focused flow can be estimated easily. However, in our study, since we work with a single syringe pump by applying negative pressure, these parameters cannot be changed during the experiment. Therefore, an equivalent circuit model is used to design the microfluidic device (Figure 3.3). With this model, an entire device and flow rates from each channel can be defined.

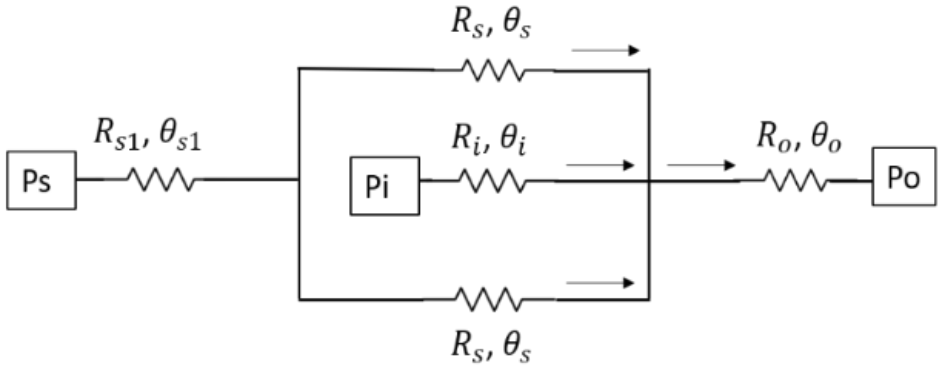

Figure 3.3 The basic analogous circuit for analyzing the hydrodynamic focusing (P_i, P_s, P_o are the pressures of the inlet, sheath, and outlet, respectively)

P_i=P_s=atmospheric pressure is accepted for the design of negative pressure devices [74]. Under these conditions, flow rates and focused flow width are determined by the hydraulic resistance as follows:

$$\frac{w_f}{w_o} = \frac{R_s}{\frac{v_f}{v_o}(R_s + 2R_i)} \tag{3.1}$$

with equivalent channel heights accepted throughout the network. Thus, the width of the focused flow can be controlled by varying the relative resistances of the side and inlet channel flows [74]. By solving the hydrodynamic focusing equations (Equation 3.1 and 2.9) analytically in MATLAB, normalized flow width at different aspect ratios can be estimated against channel resistance ratios. If the channel height is assumed to be 100 µm, the effect of the focused width (w_f) with change in the sample to sheath resistance ratio (R_i/R_s) for different outlet channel width as in the Figure 3.4.

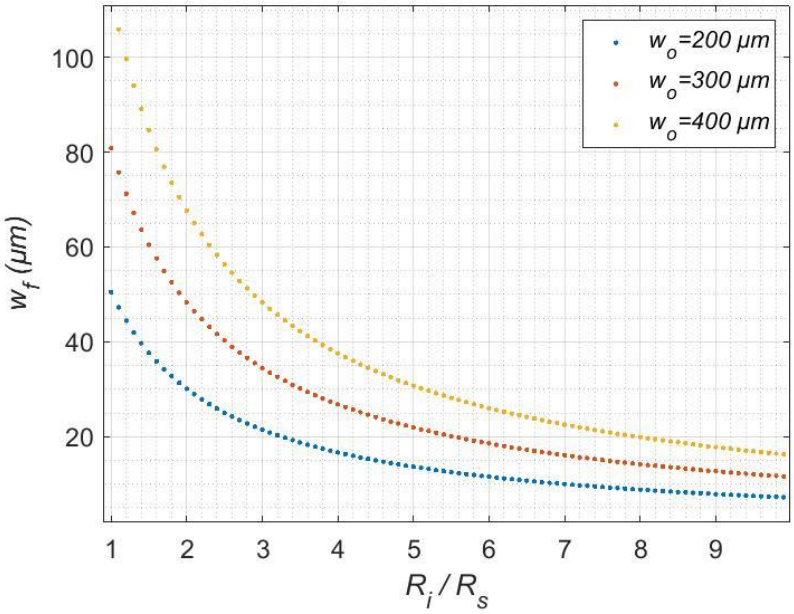

Figure 3.4 Comparison of the focused width (w_f) as a function of inlet and relative side channel resistance ratios (R_i/R_s) in microchannels with different outlet channel widths when channel height is assumed to be 100 μm

Considering the graph, if we want the focused stream width to be approximately 20 μm, the R_i/R_s ratio should be 3, 5.5, 7.5 for outlet channel widths of 200 μm, 300 μm, 400 μm, respectively. It would be necessary to increase the inlet channel resistance significantly to achieve high resistance ratios. Therefore, an outlet channel width of 200 μm was chosen with a R_i/R_s ratio of 3. In order to provide this resistance ratio, channel widths and lengths were determined with a help of the model generated in MATLAB Simulink (Appendix A). The FHR system was also added to the model (Available Atay et al. [53]) and includes all the parameters in the system. In the mathematical model, the syringe pump is modeled as a flow source, the pipe connecting the FHR and the microchannel is modeled as a resistor, and the FHR system integrated with the pipette tip is modeled as a capacitor since air is trapped inside. The microchannel structure is modeled in such a way that each channel has a different resistance. In addition, manufacturing limits and the size of the fluidic connector and reservoirs such as syringe and FHR mechanism used at the inlet and

outlet ports were also taken into account to determine the channel length. For example, there is a 5 ml syringe with a diameter of 12.06 cm at the sheath inlet, a 1 ml syringe with a diameter of 4.78 cm at the cell inlet, and an FHR mechanism with a diameter of 16.05 mm at the outlet port. In addition, channel lengths have been limited by considering the tearing and damages that the PDMS chip may cause while removing it from the mold. The total length of the channel is 36 mm.

Table 3.1 presents all related design parameters used in the proposed microfluidic device.

Table 3.1 Design criteria utilized for proposed microfluidic device

Design Criteria	**Microfluidic Device**
Number of ports	2 inlet & 1 outlet
Channel depth (sheath, inlet, outlet)	100 µm
Sheath channel width	500 µm
Inlet channel width	100 µm
Outlet channel width	200 µm
Sheath channel length	24.5 mm
Inlet channel length	7.5 mm
Outlet channel length	15 mm
Total channel length	36 mm
Mold material	Brass
Mold depth	5 mm
Mold pool length	59 mm
Mold pool width	24 mm

According to the aforementioned dimensions, the solid model of the mold was generated in Autodesk Fusion 360, as shown in Figure 3.5. The molds are designed as pockets for ease of use. The pocket depth will give the height of the PDMS chip, and the 5 mm is ideal as it will carry the reservoirs at the ports. Brass was chosen as mold material because of ease of processing and pricing factors.

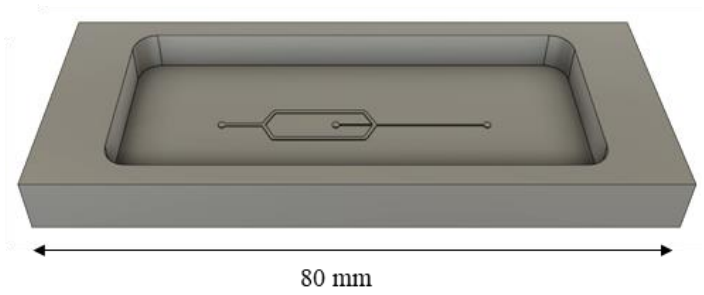

Figure 3.5 Solid model of the mold

3.2 Device Fabrication

3.2.1 Mold Fabrication

In this study, the microfluidic channel was manufactured by the micromilling method using a brass plate. The difference in micromilling compared to conventional milling operations is that the tool diameters are small, and the machining precision is high. Since the micromilling method consists of only CAD design and CNC machining, it is considerably faster than other fabrications methods such as photolithography. It is advantageous to use micromilling technique because it has faster fabrication process, lower cost and flexible method [75]. Micromilling follows design to extract the microstructure pattern at the substrate of the material, so it can be used with many different materials [76].

Solid modeling of the mold was created in Autodesk Fusion 360, which is a free CAD/CAM software for students, according to the parameters determined in the chip design section. The pool length and pool width of the mold is 62 mm x 24 mm, the pool depth is 5 mm and total height is 7 mm. The dimensions of the mold were designed in accordance with the microscope glass slide. Then, CAM codes were created in the same software. The mold was manufactured in METU Mechanical Engineering Department Micromanufacturing Laboratory with CNC micromilling machine (Proxxon MF70 CNC-ready, Wecker, Luxemburg) by Ender Yıldırım's

laboratory group. The milling process consists of 6 steps. For the milling process, 3 mm, 1 mm, and 0.2 mm diameter end mills were used, and feed rates were set to 60 mm/min, 30 mm/min, and 10 mm/min, respectively, at a spindle speed of 4000 rpm. The total machining process takes about 4 hours. The ultrasonic cleaner was used to remove thick metallic and non-metallic burrs, machining contamination, and lubricants from the surface [77]. The image of the fabricated mold is given in Figure 3.6.

Figure 3.6 Image of the brass mold fabricated by micromilling

3.2.2 PDMS Chip Fabrication

Polydimethylsiloxane (PDMS) microfluidic chips were fabricated by standard molding process. PDMS is one of the most important materials used in biological and chemical applications due to its non-reactivity, transparency, and biocompatibility [78]. Owing to its flexible structure, it can be easily removed from the mold. In addition, PDMS is a material that is very easy to prepare and can be easily bonded to glass permanently. Therefore, PDMS material was chosen for microchannel fabrication. The fabrication stages of PDMS are given in detail below (Figure 3.7).

First, PDMS and curing agent (Sylgard 184, Dow Corning) were mixed at a ratio of 10:1 in a transparent plastic cup for 5 minutes until the entire mixture was filled with air bubbles. It is important that the binder is dispersed homogeneously in the mixture. After mixing, a lot of air bubbles formed in the mixture. These air bubbles were

degassed with the desiccator. This process takes about 60 minutes. Instantly opening/closing the air vent of desiccator and vacuum accelerates the process. The mixture was poured into the brass mold, which is cleaned with N_2 gas. When the appropriate PDMS is prepared, casting the PDMS on the mold is quite simple. Since the mold used is in the pool structure, it is filled with PDMS to the brim. The mold was then placed on a flat surface and cured at room temperature for 24 hours. Curing it at room temperature for a longer amount of time might be the best way to ensure that any tiny bubbles in the PDMS do not expand. Mechanical properties and surface quality of PDMS also depends on curing temperature and duration. An alternative to low temperature curing is use of a second degassing stage after PDMS is poured in the mold. The mold used has a negative structure. The protrusions on the mold take the shape of the mold as an intrusion on the PDMS and the intrusion on the mold as protrusions on the PDMS. After curing, the PDMS was removed from the mold using a sharp razor. Then, the inlets and outlets of the microfluidic device were punched with a 1 mm biopsy puncher to allow fluid entry. Since the dimensions of the designed PDMS are the size of a microscope glass, there is no need to cut the PDMS block.

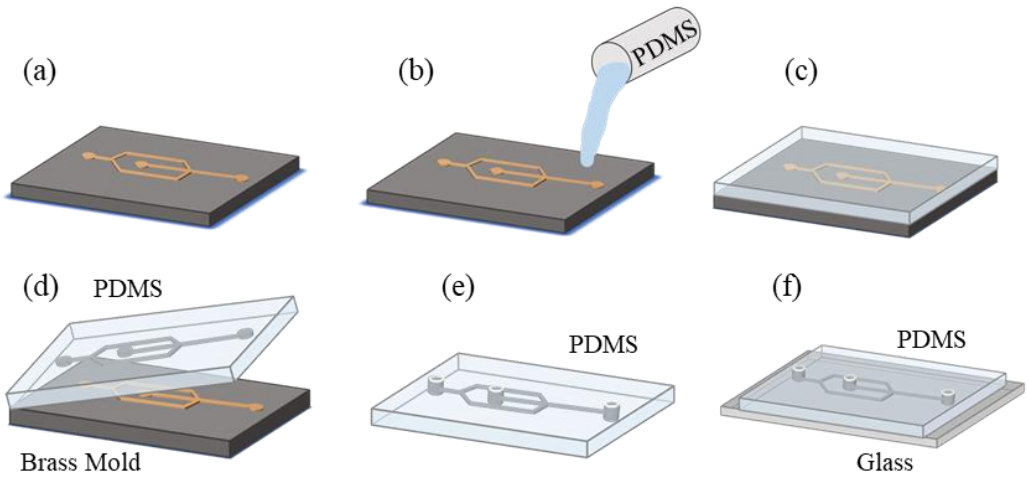

Figure 3.7 Schematic diagram of PDMS microfluidic chip fabrication: (a) Brass mold fabrication with micro milling (b) PDMS casting (c) PDMS curing (d) PDMS chip cut and peeling off (e) punching inlet and outlet ports (f) bonding to glass

3.2.3 Oxygen Plasma Treatment

The PDMS is bonded to the glass slide by the oxygen plasma treatment. When PDMS is exposed to oxygen plasma, Si-CH_3 bonds on its surface are broken and Si-OH bonds are formed. When the PDMS contacted with the glass surface, a strong covalent bond Si-O-Si is formed between the glass and the PDMS. This covalent bond between them provides a strong irreversible sealing. There is no standard protocol for plasma processing. Process parameters may change depending on the brand of plasma device and the surface roughness of the mold. Therefore, optimization of the plasma process is necessary. Three parameters are effective in plasma optimization: chamber pressure, process time, RF Power. In the optimization, the chamber pressure was kept constant, the highest quality bonding was tried to be obtained by changing the processing time and RF Power. A series of experiments were carried out to perform the PDMS-glass bonding. The optimal bonging recipe obtained with the Diener Oxygen Plasma device is summarized in Table 3.2. There was no bonding for the 'poor' parameters, while certain parts of the chip were bonded for the' partial bond' parameters. The optimal results were found with 50W RF Power, 26.6 sccm and 20 s exposure time. The PDMS chip bonded to the glass with the specified recipe was filled with a fluorescent dye. As can be seen in Figure 3.8, there is no problem in bonding since no leakage occurs into the chip.

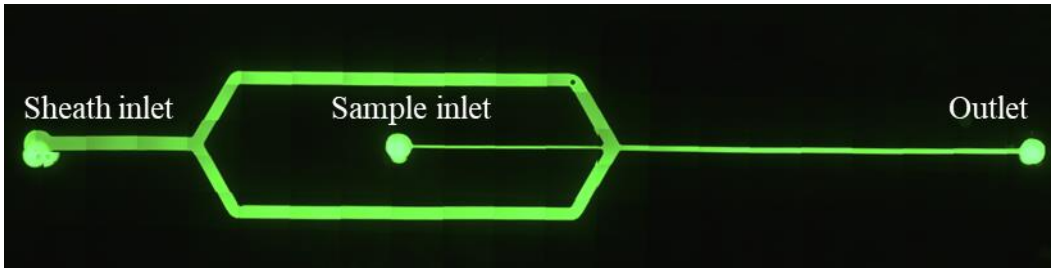

Figure 3.8 The PDMS channel was filled with fluorescent dye and monitored under a fluorescence microscope. No leakage was observed between PDMS and glass.

Table 3.2 Optimization of Diener Oxygen Plasma device

Sample	***Power (W)***	***Pressure (Torr)***	***Exposure time (s)***	***Bonding quality***
1	80	1	30	Poor
2	80	1	20	Good
3	80	1	15	Good
4	70	1	20	Partial bond
5	70	1	15	Good
6	60	1	20	Partial bond
7	60	1	15	Good
8	**50**	**1**	**20**	**Very well**
9	50	1	15	Partial bond
10	40	1	20	Poor
11	40	1	15	Very well
12	30	1	20	Poor
13	30	1	15	Poor

Before starting the plasma treatment, the glass microscope slide is cleaned of dust and impurities with IPA and dry off the isopropyl alcohol completely using the nitrogen gun. Although the plasma treatment only activates the PDMS surface, plasma treatment is also applied to the glass. Because plasma cleans the glass surface and provides a better bonding. Both parts are placed in the plasma device with the surface to be bonded facing upwards. The plasma environment is vacuumed, and oxygen gas is given to the environment at a flow rate of 26.6 sccm and treated with RF plasma for 20 seconds. It is important that the color of the plasma is purple to pink. After the oxygen plasma process is finished, PDMS and glass surfaces are brought into contact with each other immediately. In order to increase the strength of the bonding, the specimen is placed on the hot plate and pressure is applied. It is kept in this way for 30 minutes at 30°C. The final fabricated microfluidic device is presented in Figure 3.9.

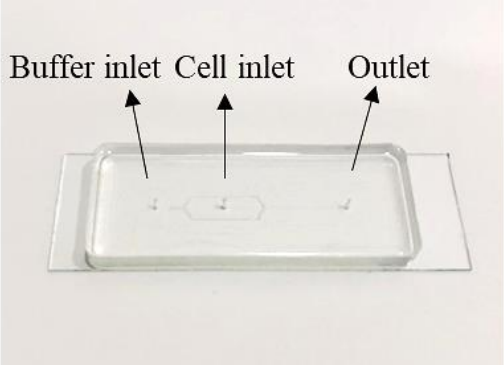

Figure 3.9 Fabricated PDMS device

3.3 Sample Preparation

Preparation of MCF7 Cells:

In this study, human breast adenocarcinoma cell line (MCF7, Leibniz-Institut DSMZ, ACC 115, Braunschweig, Germany) was used to determine the performance of the system. The preparation of cancer cells was carried out by Gizem Karayalçın in the Mikro Biyosistemler Cell Culture Laboratory. Cancer cells were cultured in DMEM medium containing 10% Fetal Bovine Serum (FBS), 1% Minimum Essential Medium (MEM) and 1% Penicillin-Streptomycin in a humidified incubator at 37 °C with 5% CO_2. MCF7s are passaged every 72 hours.

The following steps were followed for the preparation of cells before starting the experiment. When the cultured cells had 70–80% confluency, cells were detached from the flask with cell dissociation solution (Trypsin-EDTA) and resuspended in PBS (phosphate buffer solution). Approximately 5 µl of cell tracer red dye (5 µM, Invitrogen, Thermo Fisher Scientific, C34552, MA, USA) is used to stain $1x10^6$ cells/ml buffer. Prepared cells were diluted to the desired cell concentration.

Preparation of Microbeads:

The steps followed during the preparation of the microspheres are given below. Microbeads (Polysciences Europe GmbH, Hirschberg an der Bergstrasse, Germany)

were used in order to detect particles more clearly in some experiments until the validation studies of the designed system. Microbeads with a diameter of 18.7±0.73 µm were used because their size is similar to MCF7 cells. Microbeads are prepared in PBS solution. Then the desired concentration is obtained by serial dilution method. The microbeads used are fluorescently labeled and have excitation and emission spectra similar to FITC [79]. 0.5% volume of Tween 20 (Sigma-Aldrich) surfactant was used to minimize bead aggregation [80].

3.4 Experimental Setup and Test Protocol

The experimental setup is shown in Figure 3.10. It consists of a microscope, monochromatic high-speed camera, syringe pump, sheath flow assisted microchip, and FHR system. Since the liquid containing a low number of cells will be collected directly at the 200 µl pipette tip, the syringe pump (Harvard Apparatus Pump 33 DDS) connected to the FHR mechanism operates in vacuum mode. Observation of cell motions and clogging in the microfluidic channel is carried out with a microscope (Leica, DMI8) and a High-Speed camera (Hamamatsu ORCA Flash 4.0) with 5x zoom while experiments were running.

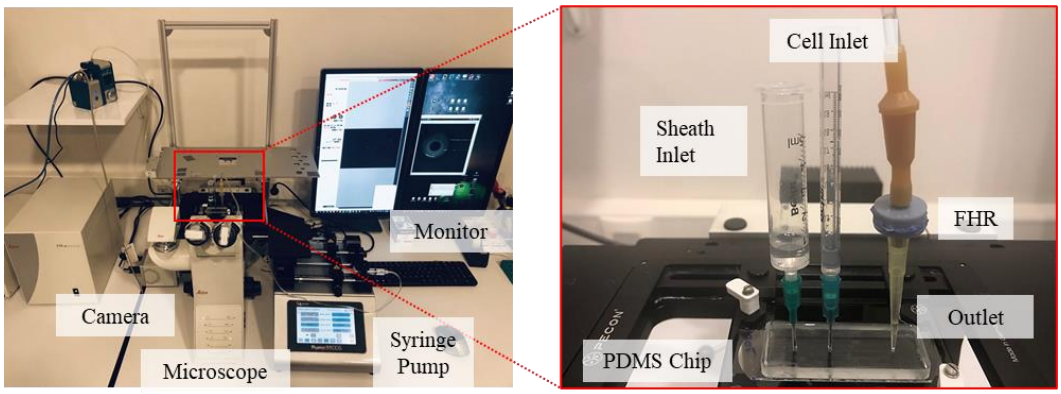

Figure 3.10 Image of the experimental setup for testing microfluidic platform

3.4.1 Device Priming

There is a certain preparation protocol for preparing microchannel before cell and bead feeding. Experimental studies were revised over time and set in concrete. Initially, PDMS channel was filled with deionized (DI) water. Thus, leaks that may also be caused by bonding at the edges and blockages in the channel are controlled. Another reason for priming with DI water is to make sure that there is no air bubble in the microchannel. After DI priming, PEG (PLL (20)-g [3.5]-PEG (2, 0.1 mg/1 ml in DI)) (SuSoS AG) coating was performed to make microchannel surface to suitable for microbeads and cells. PEG is a hydrophilic polymer and prevents cell adhesion and biofouling [81]. In the literature, PEG coating is 15 minutes for silicon microchannels [82]. Therefore, 15 minutes of PEG pre-treatment was applied. As a final step, the channel was washed with DI water and PBS.

3.4.2 Sample Processing Protocol

A syringe needle with blunt ends is used to provide fluid inlets of the PDMS device after bonding. The diameter of the punch is selected according to the diameter of this syringe needle. A needle with a slightly larger outer diameter than the puncher size should be chosen to ensure a tight connection. Therefore, 18G (0.84 mm ID/1.27 mm OD) blunt tip needle tip was selected to use at the inlet ports. The syringe needles to be used in the transfer of liquid were carefully inserted into the cell inlet and sheath inlet ports of the PDMS device. If the needles are not aligned with the punched holes while stabbing, leaks may occur on the edges of the ports. Then, the priming process explained in the previous section was applied. The PDMS chip, was placed on the microscope stage and reservoirs were attached. FHR connections were made with the syringe pump and pipette tip. The prepared sample, which may consist of cells or beads, was introduced into the inlet reservoir. PBS was given to the sheath reservoir. After determining the observation area and adjusting the focus, the flow rate was set in the syringe pump. After the targeted number of cells/beads had passed

through the observation area, the sample collected at the pipette tip was transferred directly to the well plate and counted under a microscope for comparison. The number of collected cells was compared with the number counted in real-time during the flow.

The behavior of the FHR module during the experimental process is summarized in Figure 3.11. The FHR mechanism integrated with the pipette tip at the outlet port of the chip is in the default position when the flow does not start. And the nitrile membrane between the upper and lower parts of the FHR is not deflected (Figure 3.11a). After the flow is started from the syringe pump in vacuum mode to collect cells, the membrane deflects towards the hydraulic chamber (Figure 3.11b). The maximum volume that can be induced by vacuum with FHR is equal to hydraulic casing volume. When the process is finished and the target number is reached, the flow is stopped. Later the syringe pump is started in infuse mode to release the cells and the sample collected at the pipette tip is transferred to the reservoir. The membrane is returned to its original state (Figure 3.11c).

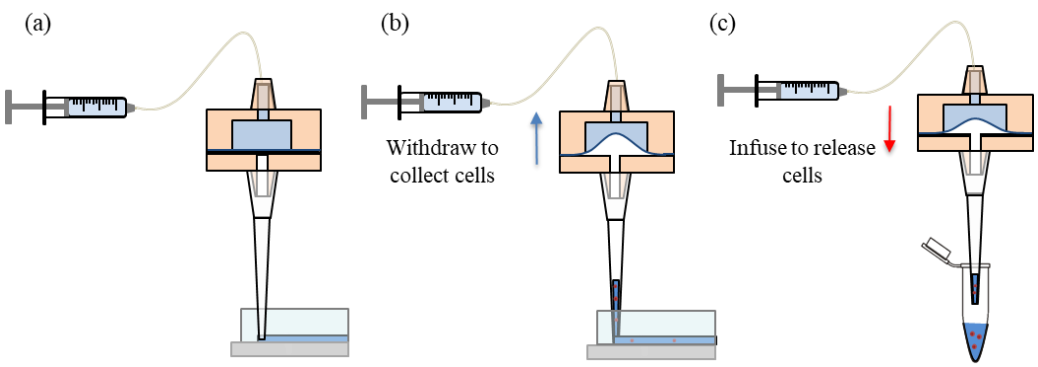

Figure 3.11 Schematic presents the operation principle of the FHR during the process. (a) initial state, (b) cell retrieval process, (c) cell transfer process

3.5 Flow Characterization Examination Method

The fluids used in microfluidic systems are transparent, such as DI water, and PBS. Therefore, in order to analyze the flow, traceable particles must be added to the

liquid. The tracer particles will depend on the characteristic of the liquid, the properties of the microchannels and the experimental technique [83]. Therefore, in the flow characterization experiments, it was decided to use microbeads with a diameter of 19 µm, as they showed a uniform size distribution and were fluorescent dyed. A microscope camera (Leica DMC5400) was used to capture and characterize the movement of particles in the microchannel. The videos recorded with the microscope were analyzed and the results were evaluated.

Two sets of experiments were carried out using the experimental setup mentioned in the previous section. In the first set of experiments, we characterize the settling time by using 1 ml and 10 ml syringes in the syringe pump. FHR with 200 µl pipette tip was used in experiments with all different syringe sizes. In the second set of experiments, the 200 µl pipette tip with and without FHR was used to understand the impact of the capacitive behavior of the FHR on the flow with the selected syringe size. Both sets of experiments were performed in the withdraw mode of the syringe pump at a flow rate of 10 µl/min.

The concentration of microbeads used as tracer particles was determined to pass 1 cell per second and was prepared in PBS buffer as described in the relevant section. High concentration makes the analysis difficult in terms of optics, while a low concentration reduces the data set point. Therefore, the optimum concentration value was tried to be obtained. In order to get video at a higher frame rate, it was recorded with 100 fps from the Leica Microscope software (LAS v4.12). The observation area was determined to be close to the outlet port and did not change during the experiment. The focus of the beads was also adjusted at the beginning of the experiment. The movements of the beads passing through the observation area and accelerating over time were monitored with a microscope. After the flow stabilized, the flow rate in the syringe pump was set to zero. Videos of microbeads flowing through the microfluidic channel with different velocities were recorded until no bead was seen in the channel. For the first set of experiments, the same steps were repeated using different sizes of syringes (1 ml, 10 ml) in the syringe pump.

Microbeads movements were analyzed using the Manual Track plug-in in ImageJ software. This plug-in allows the user to quantify the movement of objects between frames of a temporal stack in 2D [84]. Before using the Manuel Track plug-in, the experimental recordings were split into frames in the VirtualDub program and saved as image sequences and imported into ImageJ software. Brightness and contrast were adjusted on the image stack. When the beads move in the microchannel, they lengthen in the direction of movement, and they appear as a rectangle. The front part of the beads was followed. The tracking was done by clicking on the starting point of the line (bead). After each mouse click, the following image of the temporal stack is activated. This plugin creates a results table (Figure 3.12) showing the pixel distance traveled of the object during the time interval between two consecutive images. This resulting table is saved in the excel document for post-processing. The same steps are applied to the videos recorded in each set of experiments.

A code was generated in MATLAB to determine the average velocity of the microbeads from the obtained data. This code calculates the average velocity in pixels/second for particles, using the time interval and the distance traveled between each frame. Using the calibration scale of the microscope, the velocity value was converted to the mm/s and then to the flow rate in μl/min, which depends on the channel geometry to be able to compare more easily with the value set in the syringe pump. With the effect of Poiseuille Flow in a microfluidic channel, the maximum velocity is seen in the middle plane of the channel and is 1.5 times the average velocity [85]. The movements of the particles passing through the central axis were followed in the analysis, and then correction was made for the average flow velocity. The average velocity of the beads passing through the observation area every 5 seconds was plotted depending on time. Since the obtained data set was very noisy, the smoothing process (moving average) was applied to the graph in MATLAB.

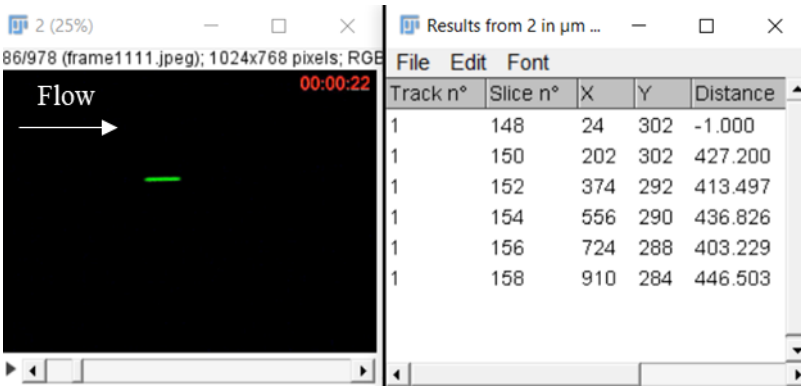

Figure 3.12 ImageJ generated table showing the results of the particles traveled during the time interval between two consecutive images. The green line is the fluorescently stained bead.

In the second set of experiments, the operation was performed with a bare syringe pump in the same setup and the results were compared with the FHR mechanism. Luer-end tubing is attached directly to the pipette tip and inserted into the outlet port of the chip. Videos of the microbeads were recorded, and their analysis was performed using the same steps explained above. Second sets of experiments were repeated three times to increase the reliability of the results.

3.6 Viability Analysis

Since the cells are affected by the hydrodynamic forces during their moving through the microfluidic channel, determining the viability of the cells at the end of the process is essential. For this purpose, the automated cell counter (BioRAD TC20, Hercules, CA, USA), which can provide viability and histogram information, was used. The cell counter can operate in the cell concentration range of $5x10^4$ – $1x10^7$ [86]. In the experiments, MCF7 cells were suspended in PBS. Since the outlet concentration will be diluted with PBS because of sheath flow, the inlet concentration and the process time was adjusted to count the collected cells with automated counter. PBS from the buffer inlet and suspension with $1x10^6$ cells/ml

concentration from the sample inlet was fed into the channel at a flow rate of 5 µl/min for 20 minutes.

Before 1 ml of sample was fed into the channel, 50 µl of the cell suspension was separated. Cells collected in a 200 µl pipette tip at the outlet and the cells in the inlet were analyzed. Cell enumeration and viability analysis were performed with an automated cell counter by mixing 10 µl of cell suspension with 10 µl of Trypan blue (0.4%, Sigma-Aldrich, T8152, Darmstadt, Germany). 10 µl of this mixture, which was prepared at a ratio of 1:1, was taken and loaded into disposable cartridges. Viability of cells is determined with Trypan blue by labeling dead cells exclusively. Because the cell membranes of live cells are intact, trypan blue cannot pass through the living cell membrane and get into the cytoplasm. On the contrary, the trypan blue penetrates the porous cell membrane in a dead cell, enters the cytoplasm, and the cell appears completely black [87]. Thereby, the device only detects live cells with a dark wall and a white inside. As a result of the analysis, the TC20 cell counter gives the concentration information of dead and live cells. For each data point, 3 counts were performed, and the average of the values was taken.

The viability value was obtained by dividing the viable cell concentration by the total cell concentration, as in the formula given below, and the viability of the inlet and outlet samples were compared with each other.

$$Viability\ (\%) = 100\left(\frac{Live\ cell\ count}{Total\ cell\ count}\right) \tag{3.2}$$

3.7 Cell Counting Algorithm

In this thesis, we propose a method that includes cell counting to determine the cell number in real-time. The aim of the proposed algorithm is to count the cells in the liquid flowing from the microfluidic channel. The used algorithm comprises image acquisition, preprocessing, segmentation, contour extraction and counter task. The entire processing flowchart is shown in Figure 3.13.

In this study, Python programming language and OpenCV (Open-Source Computer Vision Library) environment were used as computer-aided image processing systems. The open source OpenCV library is freely accessible to everyone was developed by Intel and is used in many Computer Vision applications today. OpenCV is a multifunctional image processing library; instead of rewriting the image processing stages from scratch, using OpenCV open-source library provides faster coding. It is mostly based on real-time vision implementations [72].

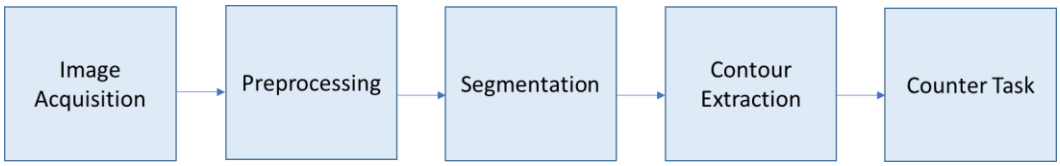

Figure 3.13 Entire workflow of the algorithm

If we want to summarize the main topics of the image processing system shown in Figure 3.13, first, frames are taken from a certain area of the screen, and a median filter is applied to the frames to reduce noise. A threshold value is then determined for cell segmentation. Objects are distinguished from the background by the segmentation step. Center points and borders of the detected contours are determined. Finally, the counter is activated according to the objects passing through the counting line.

3.7.1 Image Acquisition

The most important part of the algorithm is image acquisition because it provides input to the algorithm. Since we want to count cells in real-time, taking snapshots of the screen is the simplest method. A fluorescence microscope is used to observe the inside of the microchannel and to zoom in 5X on the cells. An Hokawo ORCA-Flash4.0 LT+ CMOS high-speed camera is mounted on the microscope and the images taken by the camera are transferred to the computer. The camera software uses the live view of the microscope.

The image viewed on the Hokawo camera is shown in Figure 3.14. The light beam at the edges and around the port creates counting errors. For this reason, the channel and its surroundings were not taken into account during image processing, but the region where the cells passed when entering the outlet port was focused on (Figure 3.15). The outlet port is only a small part of the region monitored by the camera. This area can be considered a pool. When the vacuum-extracted cells arrive at the port, they rise towards the pipette tip. As they get farther away, their brightness gradually decreases, and they grow and disappear. In Figure 3.15, an example of the captured image for processing in real-time is given. The cropped image has 250x250 pixel size. Our algorithm starts by taking snapshots from certain pixels of the screen (outlet port) and reading the frames. 30 fps frame rate was achieved with screen capturing method. After this step, image processing begins.

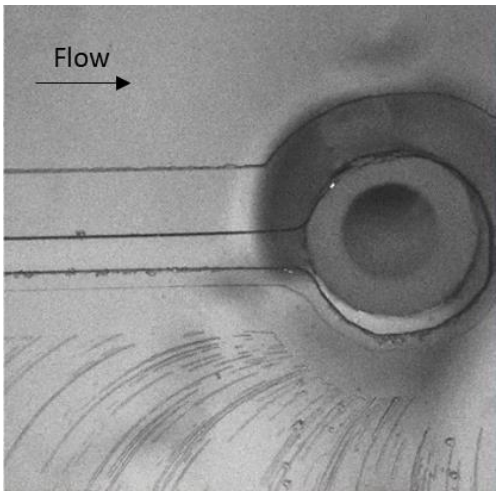

Figure 3.14 Microchannel image viewed by ORCA-Flash4.0 LT+ camera

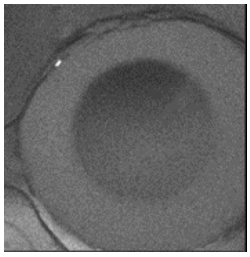

Figure 3.15 Cropped image for image processing

3.7.2 Image Preprocessing

The objective of the preprocessing step in an image processing program is to improve image quality or to enhance the image. Within the scope of this process, converting images to gray format and filtering steps are applied.

The condition of the working system is as follows: There is a stable fluorescent source. Thus, the stained cells in the channel can be distinguished from the background under a fluorescent microscope. The only detectable objects that move in the stream are the cells. First, the RGB format in each frame is converted to gray scale. In the next stages, the processing is carried out in gray format. A grayscale digital image consists of a single sample carrying only intensity data. This type of image, often known as black-and-white, consists solely of grayscale tones, ranging from black at the lowest intensity to white at the highest [88].

Noisy parts in the images may lead to incorrect results during the operation of the algorithm. Therefore, it should be reduced and eliminated. It will also help improve image quality for further processing. The median filter was chosen due to its ease of application and shortening of the processing time. The median filtering method is a basic nonlinear smoothing technique.

3.7.3 Segmentation

After the preprocessing steps, the segmentation phase begins to extract the background. After the preprocessing stages to clear the background images, the segmentation phase begins. Segmentation is often used as a way to select areas of interest for an image. As a result, with a simple segmentation technique, objects are separated from the background, and their detection becomes easier.

Thresholding, which converts grayscale images to binary images, is the most effective and easiest way to separate objects from the background [89]. The global thresholding method is used for the segmentation of cells because of its simplicity

and effective results. As a result of the thresholding process, a binary image is obtained. In this method, a threshold value must be determined between the cells and the background. But finding a constant value for each cell and for each condition is quite challenging because not all cells have the same intensity. Thus, some particles passing through the observation area may not be counted. In addition, cells can be damaged and destroyed during the preparation process of the sample. In such cases, fragments and dye residues show fewer intensities than normal viable cells. Such low brightness should be ignored during counting. The selected threshold value should separate each cell from the background and should not be affected by the surrounding shadows. Apart from that, since the system is not enclosed and the PDMS material is transparent, the camera may be affected by the light beams from outside. To overcome such problems, the thresholding method is useful. As a result, 140 pixel was accepted as the threshold value. This value is adaptable in most cases, but a pre-run is required before the sample retrieval process. Threshold value can be set during pre-run trial. Pixels smaller than the threshold value are background, while larger pixels are segmented as white and represent the cells, as shown in Figure 3.16.

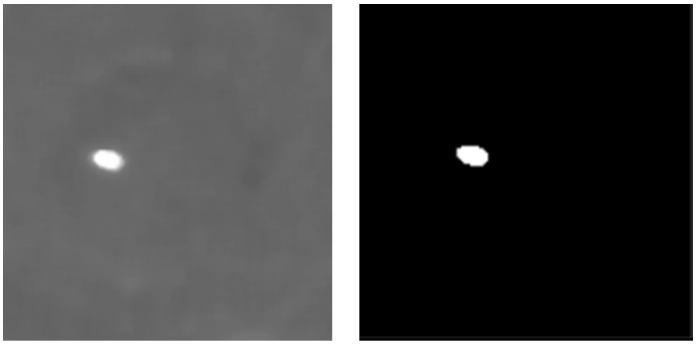

(a) (b)

Figure 3.16 (a) Filtered image and (b) segmented image. The white parts represent the cell while the gray parts represent the background. (Threshold=140 pixel)

With thresholding, the edges of the object in the image are turned completely white, so the algorithm can now detect the boundaries of objects from these white pixels. Contours are a curve that connects all continuous points of the same color and density

along the border and represents the shapes of objects in an image [90]. The contours in each frame are assumed to be cells. In order to obtain the position information of the contours, the bounding box is drawn to the contours. Bounding box is the rectangle shape drawing that includes whole object. It is updated at each step and useful for visualization. Centroid of the bounding box shows the last position of the object and updated at each step. Basically, the counting algorithm is based on the comparison of the centers of the bounding box in each frame. By calculating the center points and areas of the contours, particles smaller than the determined area are not counted. Thus, unwanted noises in the system are also eliminated with the cross-check.

3.7.4 Counting Task

The counting algorithm is quite simple because objects are moving in the same direction with the flow. Detection of moving cells is achieved by comparing the centroids of the targets found in two consecutive fluorescent images. A counting line is created perpendicular to the direction of movement of the cells. The counter is activated when the center point of detected cells crosses this line as seen in Figure 3.17.

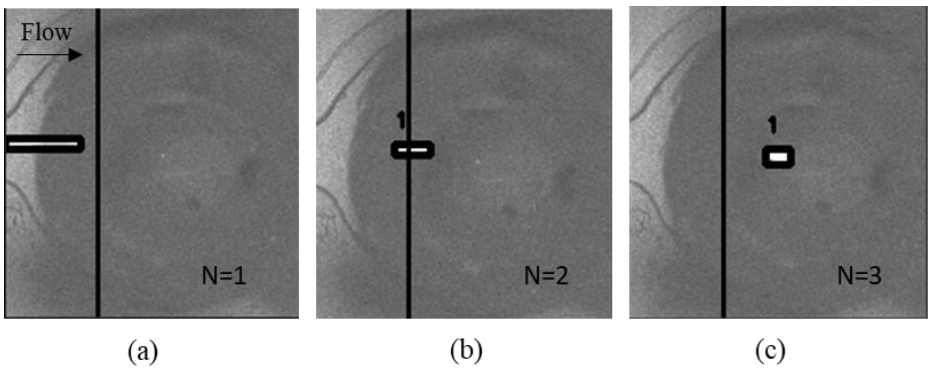

Figure 3.17 Cell counting process: a) Before the centroid of the target object crosses the counting line, counter is zero. b-c) After the centroid of the target object crosses the central line, the algorithm counts the cell. Cells are shown white, the black rectangle is the bounding box.

When a contour enters the frame, it first stays to the left of the line. It crosses this line as it moves in the direction of the flow. This can be accomplished with a simple loop by calculating the distance of the contour centers to the horizontal line. However, this algorithm does not give correct results in the case of two cells being consecutive. The flowchart of the algorithm is given in the Figure 3.18.

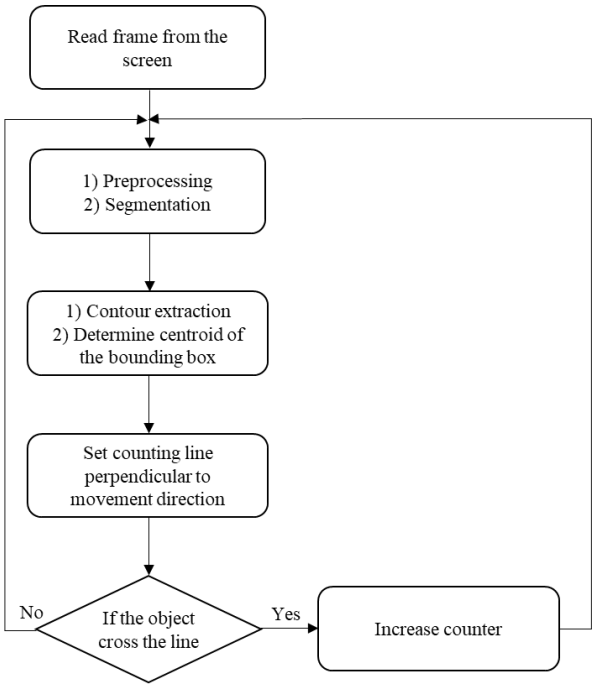

Figure 3.18 Flow chart of the cell counting algorithm

CHAPTER 4

RESULTS AND DISCUSSION

4.1 Flow Characterization Results

To determine the effect of syringe size on flow, we characterized the settling time using different sizes of syringes (1 ml, 10 ml) with FHR connected microfluidic platform. The flow examination method is explained in the Chapter 3.5. Briefly, we calculate the pixel difference between consecutive frames and divide by the time interval. The results are presented Figure 4.1. Moving average filter on MATLAB was applied to the raw results.

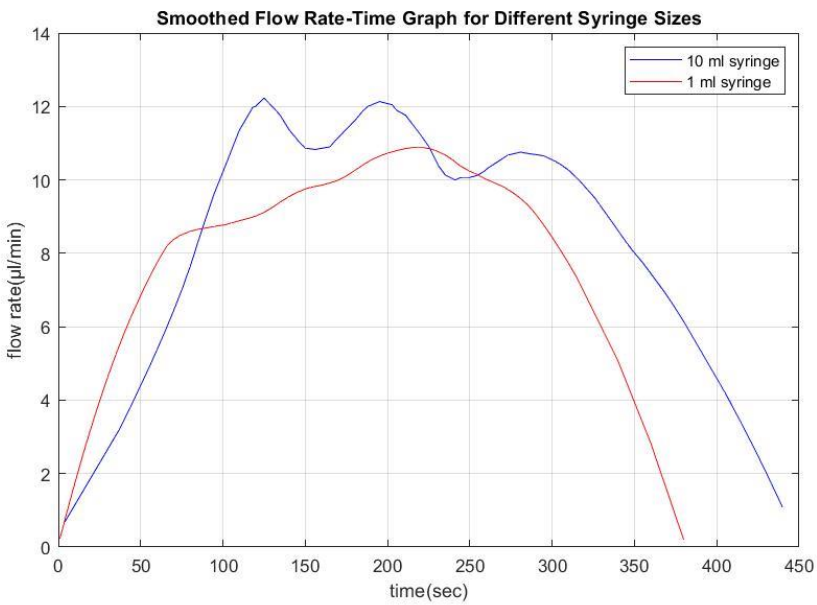

Figure 4.1 Effect of different syringe sizes on flow in microfluidic system with FHR. The graph is plotted against the flow as a function of time.

According to the graph, there are more fluctuations with 10 ml syringes. This is an expected scenario. Since the piston's displacement and the injected volume are

correlated, this small movement results in a minimal injected volume. Therefore, discrete phenomena appear as periodic oscillations or pulses because of motor steps. The minimal injected volume is proportional to the syringe diameter [91]. That's why a smaller syringe size recovers flow stability. As a result of this set, it was decided to continue with a 1 ml syringe.

In addition, a series of experiments were performed to characterize the flow response of the FHR within the scope of the second set of experiments. Two cases, FHR with a pipette tip and bare syringe pump with a pipette tip, were simulated to demonstrate the effect of trapped air on the performance of FHR. Since noise caused by the measurement method was observed in the data set, the results are presented by taking the average of three experiments and smoothing the graph. The plot would benefit from some indication of the standard deviation arising from variations in the three experiments. Smoothing was carried out in MATLAB with a moving average filter. The 10% envelope around the flow rate value is given by the dotted line. Behavior of the FHR mechanism and bare syringe pump are shown in Figure 4.2.

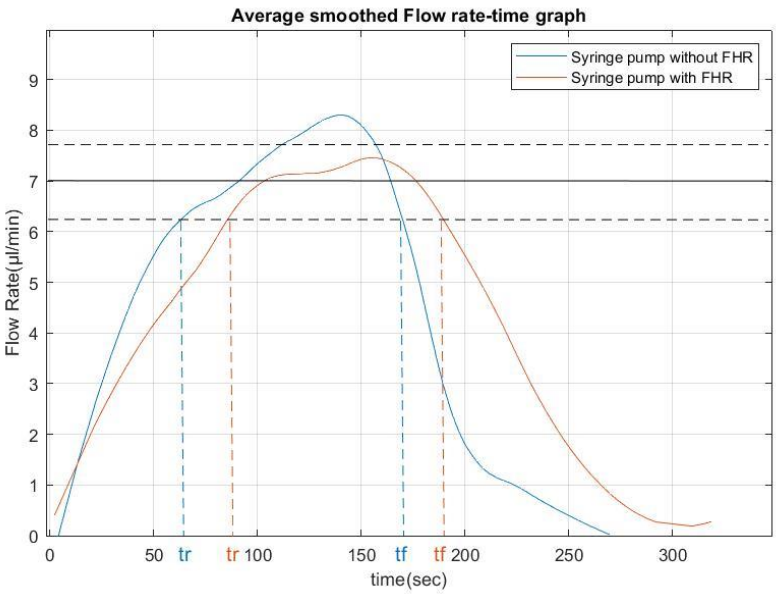

Figure 4.2 The graph shows the flow rate as a function of time for a bare syringe pump with a 200 µl pipette tip and FHR with a 200 µl pipette tip.

As can be seen from the graph, the FHR has a longer transient response due to the capacitive behavior caused by the trapped air. According to the graphs, while the flow stops in 280 seconds without FHR, it lasts for 320 seconds with the FHR effect.

Rising and falling times have also been determined in order to characterize the behavior of FHR. These values are the time to reach 90% of the target flow rate as the flow increases and decreases, respectively. The difference between the rising time of the bare syringe pump and the FHR is 25 seconds, and the difference between the falling time is 19 seconds. This numerical result also confirms that the capacitive effect of FHR on the syringe pump is not significant. In addition, more fluctuations were observed in the results without FHR on the raw data. This is due to the damping effect resulting from the capacitive effect of the FHR [53].

4.2 Hydrodynamic Focusing Verification

It was aimed to verify the focusing on the fabricated PDMS chip. The sample is compressed in the middle of the channel by applying sheath flow from the side channels according to the principles of hydrodynamic focusing. Since the average cell diameter is 14 μm, the calculations were carried out accordingly. In order to observe the predicted hydrodynamic focusing effect in the main channel, the flow behavior was observed under an inverted microscope. While DI water is used at the sample inlet, fluorescent dye-stained DI water is used in the buffer inlet to see a clear distinction. Flow rates of 50 μl/min were set in the syringe pump placed at the outlet port with FHR, and the focused flow behavior was examined under the microscope. Then, images of the main channel were taken by Leica software (LAS v4.12) and the focused flow width was determined by using the scale bar on the acquired image. Figure 4.3 shows the result with a scale bar on the pinched solution.

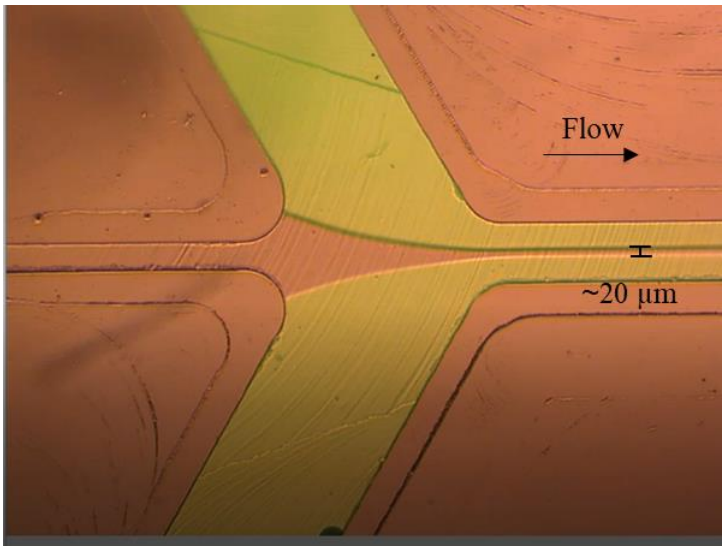

Figure 4.3 Experimental effect of the hydrodynamic focusing with 50 µl/min negative flow rate (Q_s/Q_i=3)

Figure 4.4 shows that MCF7s are focused along the center of the outlet channel under a flow rate of 5 µl/min.

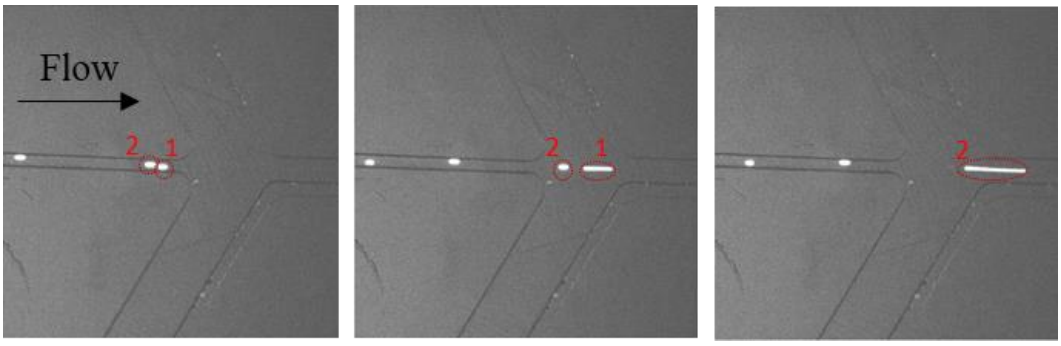

Figure 4.4 Experimental images of the cells moving through the focused stream under 5 µl/min flow rate (Q_s/Q_i=3)

4.3 Flow Rate and Concentration Results

In cell enumeration systems, there are two important parameters that affect the performance of the system: flow rate and concentration. Finding the optimum values of these parameters is important in terms of testing the operability of the system. A series of systematic experiments were conducted to determine the performance of

the system using different concentrations of MCF7 cells and different flow rates. Initially, experiments were carried out at different flow rates between 1 µl/min and 15 µl/min at $1x10^6$ cells/ml cell concentration.

Particle velocity, which depends on the channel geometry and flow rate, has a tradeoff relationship with the image quality. As the particle flow velocity increases, the blur caused by the motion occurs [92]. However, as the particle flow velocity decreases, the throughput of the system reduces while obtaining a higher image quality [93]. Since the aim of this study is to count cells with the highest accuracy, throughput was not taken into consideration. A constant flow rate is not very critical in the proposed microfluidic platform. Since the aim is to monitor the cells passing one by one, the system cannot be operated at a high flow rate (over 10 µl/min). There is no problem in operating at any value in the low flow range where the cells can be determined while moving. However, an operation flow rate value has been determined to optimize the duration of the process and concentration and provide ease of operation of the system. As a result of the experiments, the 5 µl/min was chosen as the operation flow rate, at which the particles could be seen clearly in microscopic examinations. Particle velocity is 4.17 mm/s at the 5 µl/min flow rate. Sequential channel views showing beads passing through the channel and processing to the outlet under 5 µl/min are given in the Figure 4.5.

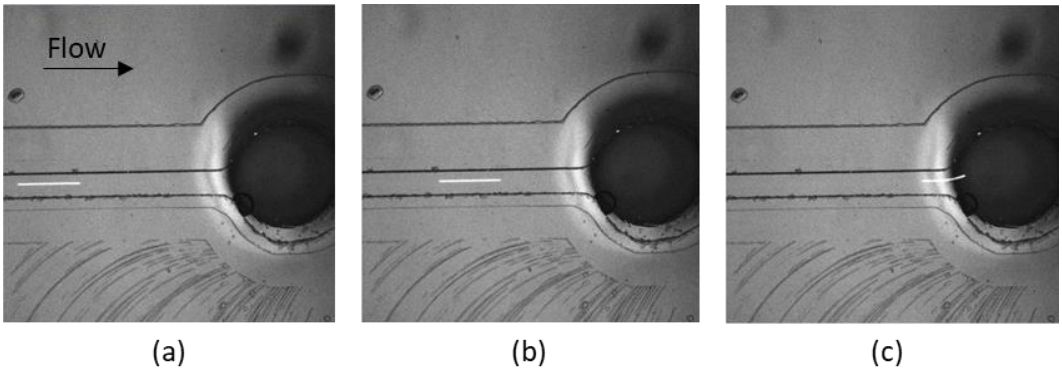

Figure 4.5 (a-c) Image of stained MCF7s passing through the channel. (Flow rate=5 µl/min, Particle velocity= 4.17 mm/s)

Another parameter that affects the performance of the system is the cell concentration. When the concentration decreases, the collection time of the targeted number of cells increases. For this reason, we tried to find the optimum concentration value at which cells can be counted one by one while passing through the channel and to estimate the concentration range in which the platform can work.

A series of experiments were performed by targeting 10 and 100 cells and determining the number of cells collected at the outlet with three different concentrations ($1x10^4$ cells/ml, $5x10^4$ cells/ml and $1x10^5$ cells/ml) under the determined flow rate. In order to find the number of collected cells, the sample at the pipette tip was transferred to the well plate and counted under the microscope. Experiments were carried out in five replicates for both targeted cell numbers, and average retrieval rates were given with standard deviations (STD).

The ratio of targeted/collected cells versus the concentration for two different retrieval number is given in Figure 4.6. The ratio of targeted/collected is presented by taking the average of the experiments performed at each concentration.

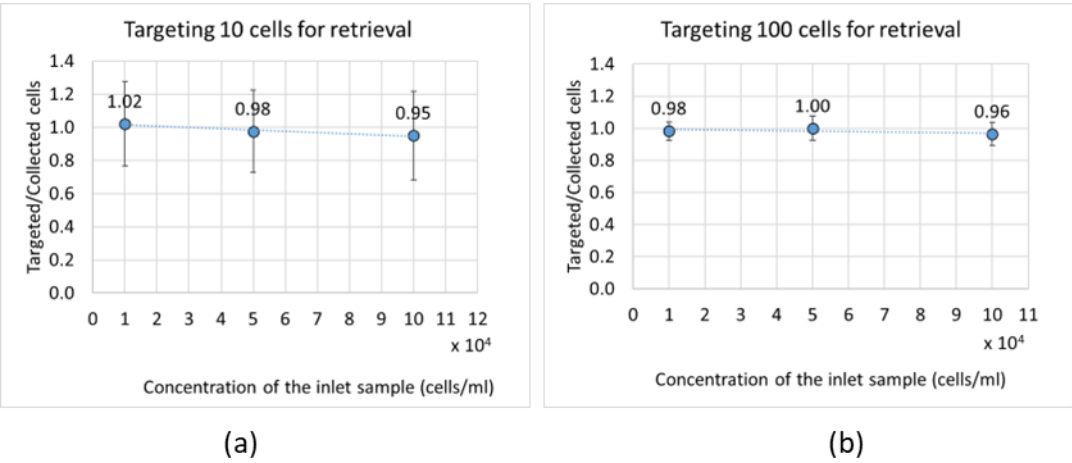

(a) (b)

Figure 4.6 The rate of targeted/collected obtained at different concentrations when (a) 10 cells are targeted to spike (b) 100 cells are targeted to spike

Firstly, as shown in Figure 4.6a for 10 cell retrieval, 1.02±0.26, 0.98±0.25 and 0.95±0.27 targeted/collected ratio were obtained for $1x10^4$, $5x10^4$ and $1x10^5$ cells/ml

concentration, respectively. According to the obtained data, it is seen that the ratio deviates from the normalized value of 1 (optimum value) as the cell concentration increases, which is an expected outcome. Because when the cell concentration increases, the number of cells passing in a minute increase, and it becomes difficult to control the system. When the pipette was pulled at that instant, the cells remained in the port because they did not fully settle on the pipette tip. Therefore, the flow is stopped and the cells are settled on the pipette tip. Since the flow cannot be stopped on time due to the long response of FHR, more cells are collected than targeted. This causes the rate to deviate towards values less than 1. However, there is no significant difference between the standard deviation of each cell concentration. The obtained results prove that any concentration in the range of $1x10^4$ - $1x10^5$ cells/ml can be studied when retrieving 10 cells. But more accurate results are achieved at $1x10^4$ cells/ml concentration. Considering the processing time, the theoretical calculation and the experimental calculation are not consistent with each other, and the time needed to collect 10 cells at $1x10^4$ cells/ml concentration is average 10 minutes from the moment of flow started. This total process time includes the time for cells to enter the channel.

Secondly, the ratio of targeted/collected cells at different concentrations for 100 cells retrieval is shown in Figure 4.6b. For 100 cells retrieval, 0.98±0.06, 1.00±0.08 and 0.96±0.07 ratios were obtained for $1x10^4$, $5x10^4$ and $1x10^5$ cells/ml concentration, respectively. Similar to 10 cells, the ratio decreases below 1 as the concentration increases except for $5x10^4$ cells/ml concentration. But this decrease is relatively less compared to 10 cells. In addition, the standard deviations were lower compared to the results of 10 cells. This shows the challenge of working with low-concentration cells. The results for 100 cells prove that system can work with high accuracy at each concentration within this range. However, when considered in terms of time, it is very time-consuming to work at $1x10^4$ cells/ml concentration. Therefore, it was decided that the ideal concentration on collecting 100 cells was $1x10^5$ cells/ml. When this value was selected, the average processing time was 10 minutes.

As a result, time optimization was also carried out with concentration adjustment. Basically, when cells are prepared at a concentration of 1000 times the targeted number of cells, the processing time is approximately 10 minutes. The collected volume is 50 µl on average. This volume includes the PBS volume from the sample inlet before cells enter the channel and the addition of sheath fluid during hydrodynamic focusing.

4.4 Viability Analysis

It is critical to determine whether cells retrieved from the device were damaged as they passed through the channel or entered the ports through the connectors. For this purpose, repeated experiments were carried out to determine the viability analysis of the cells. The cells can be damaged due to the placement of the needle tip and pipette tip in the inlet and outlet ports of the PDMS chip. When inserting the connection elements into the ports of the chip, there must be a minimum distance from the bonded glass slide. This should be taken into account during experiments. The viability of the cells fed to the channel at the sample inlet and the cells collected at the outlet is given in Table 4.1. The results prove that the cells remained viable and healthy after the process.

Table 4.1 Viability of cells retrieved from the outlet after process

Viability (%)	***Inlet***	***Outlet***
Exp #1	92.1	89.2
Exp #2	94.1	88.5
Exp #3	91.1	83.4

Viable cells were also confirmed by optical examination of retrieved MCF7 cells. An example image from the cells collected in the well plate is given in Figure 4.7. The cells collected at the outlet appear mostly intact and circular.

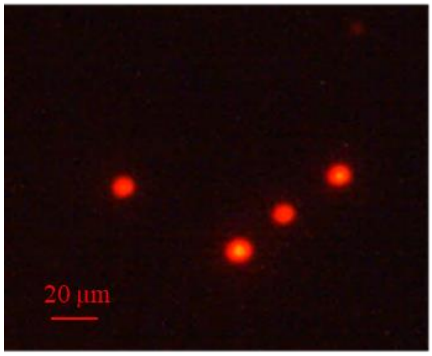

Figure 4.7 Fluorescently stained MCF7 cells were intact in the 96 well-plate after process

4.5 Performance Experiments

After several experimental parameters, including the concentration and flow rate were determined, the performance evaluation studies started. To validate the proposed device, experiments were conducted using two different sample solutions: 1) microbeads for accurate control of particle loss to quantitatively assess accuracy, and 2) real cell line to verify its feasibility for practical biological applications. Performance tests of the proposed microfluidic platform were performed manually (visually) without using the real-time counting algorithm.

4.5.1 Validation with Microbeads

Fluoresbrite® YG Microspheres beads with a diameter of 19 µm, which are similar to the diameter of MCF7 cell lines to be used in validation with live cell experiments, were chosen for the validation of the system with microbeads. The purpose of these experiments is to determine the particle losses that may occur in the microchannel and connection elements, and to evaluate how accurately the particles counted in the microchannel are retrieved from the outlet. In this study, the advantage of using microbeads instead of cells is to minimize external factors. Because microbeads are made of polystyrene, are solid structures, and they all give the same brightness due

to internally dying. Therefore, experiments with microparticles were first performed to determine the accuracy of the system. The retrieval accuracy was calculated with the following formula. This ratio should be close to 100.

$$Counting\ accuracy\ (\%) = 100\left(1 - \frac{|\#of\ retrieved\ particles - \#\ of\ counted\ particles|}{\#\ of\ counted\ particles}\right) \quad (4.1)$$

The number of beads passing through the channel and the number of beads collected at the outlet to was used to determine the counting accuracy. From 1 to 60 beads were randomly passed through the channel without specifying the target number. The results obtained from different measurements are presented in Figure 4.8.

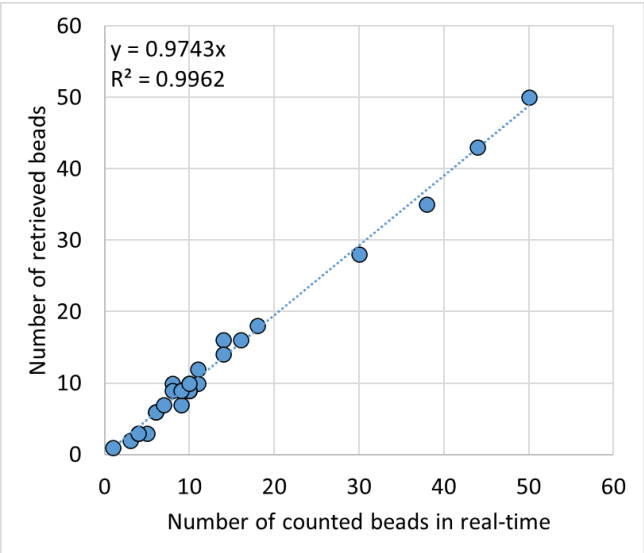

Figure 4.8 Regression analysis of the number of collected beads within the well plate versus the number of beads counted in real-time between 1-60 cells

Using Equation 4.1, the average counting accuracy was calculated for 29 different experiments. As a result, the counting accuracy value was found to be 90.95%±11.22%. The retrieval of less beads than counted in the microchannel indicates that the particles remain in the outlet port or are lost in the connection components, and this is a predictable scenario. However, collecting more beads than

counted is an abnormal result. This is thought to be due to the chip not being cleaned well. Different PDMS devices are not fabricated for each trial; sometimes, sequential measurements may be taken in the same device. Regression analysis was also performed to see the linearity of the system. The repeatability of the data is high (R^2>0.99).

As a result, the obtained data with microbeads show that the applied protocol work as intended. For this reason, validation studies were carried out with real cancer cells in the next step.

4.5.2 Validation with Cells

In the validation experiments with cells, live breast cancer cell lines were used. The cultured cells are prepared at the desired concentration by serial dilution method. It was targeted to collect cells at certain values (10-50-100 cells) in the experiments to determine the accuracy of the proposed setup. The accuracy was calculated by comparing the value of cells received at the pipette tip with the value of the cells targeted to collect. Cells passing through the observation area of the chip were counted visually in real-time to obtain the targeted number. The same experimental parameters were used as validation with microbeads. 30, 15, and 16 measurements were taken for 10, 50, and 100 retrieval rates, respectively. The following formula was used to determine the retrieval accuracy of the microfluidic system:

$$Retrieval\ accuracy\ (\%) = 100\left(1 - \frac{|\#of\ retrieved\ cells - \#\ of\ targeted\ cells|}{\#\ of\ targeted\ cells}\right) \quad (4.2)$$

The mean values of the collected cells for each retrieval cell number are summarized in Figure 4.9a. Data represent the mean of experiments performed at each targeted number. The average retrieved cell count was 9.2±2.4, 49.4±5.9 and 98.5±6.2, with the target of collecting 10, 50 and 100 MCF7 cells, respectively. In addition to

experiments targeting 10, 50 and 100 cells, single-cell-retrieval was also tested. A total of three experiments were performed targeting 1 cell. In each of these 3 experiments, 1 cell was successfully collected at the pipette tip.

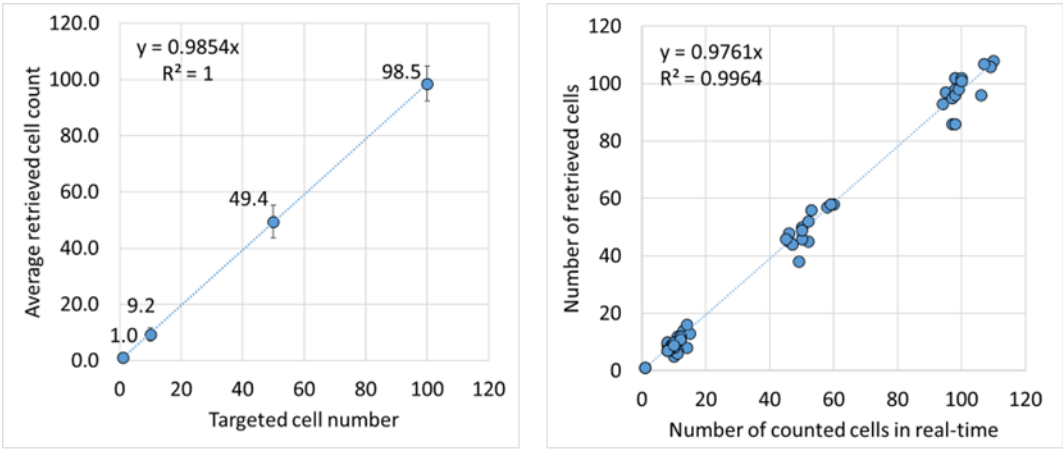

(a) (b)

Figure 4.9 (a) The average cell count versus the number targeted cells to be spiked (b) Regression analysis of the number of collected cells within the well plate versus the number of cells counted in real-time at 3 different cell number point

Using Equation 4.2, retrieval accuracy rate was calculated, which shows the value of how accurately we can collect the target number. The average number of retrieved cells, and the accuracy rate are summarized in the Table 4.2.

Table 4.2 Average retrieved cell count and retrieval accuracy parameter calculated at three different targeted cell number

Number of Targeted Cells	***Average Retrieved Cell Count***	***Retrieval Accuracy***
10 (n=31)	9.2±2.4	82.3±10.5%
50 (n=15)	49.4±5.9	90.0±6.2%
100 (n=16)	98.5±6.2	96.7±5.6%

While trying to collect the targeted number, some errors occur during synchronous visual counting, such as the inability to determine the exact number because the cells moving together. For this reason, in addition to real-time visual counting to achieve the targeted number, the video of the observation area was recorded during the process. After the experiment, the video was examined and the exact number of cells passing through the channel was determined visually. Figure 4.9b shows the linear regression between the number of counted cells from the video and the number of retrieved cells. This data shows that the system can be operated to receive 10-100 cells with high linearity ($R^2 > 0.99$).

The obtained performance parameters are comparable with other microfluidic cell isolation methods. Ding et al., proposed a retrieval method for single-cell detection using a static droplet array (SDA) microfluidic device. Retrieval process takes less than 15 min. They used MCF7 cells at $5x10^3$ cells/ml concentration to determine the performance of the device. Cell transfer rate was found to be 80%. Since the device has 240 pockets, the retrieve number is between 1 to 240 [8]. Chen et al. developed a single-cell detachment method to collect cells. They loaded MDA-MB-231 cells into the microfluidic chamber at a concentration of $1x10^6$ cells/ml. The cells were adhered onto the substrate then laser pulse was applied to detach the cells. The collection rate of detached cells is more than 90%. The viability of the cells was found to be 83% [10]. Yusof et al., reported a method to isolate single cells encapsulated in a droplet. Cells prepared at a concentration of $5x10^5$ cells/ml were supplied to the chip and approximately 50 cells were targeted for transfer. With this method, 87% collection efficiency and 75% viability were obtained [49]. Tokar et al., reported a microwell array for single cell transfer. After determining the target cells with a microscope, they are aspirated into the glass pipette tip from the microarrays. 85-95% transfer efficiency was achieved. Total transfer time was 10 minutes on average [52]. Table 4.3 presents the performance parameters of the device in the literature and this study as a comparison.

Table 4.3 Comparative table of single-cell isolation methods available in the literature

Study	Cell concentration	Retrieve number	Accuracy	Viability	Time
Ding et al. [8]	$5x10^3$ cells/ml	1-240 cells	80%	86%	<15 mins
Chen et al. [10]	$1x10^6$ cells/ml	1-1000 cells	>90%	85%	24 hours
Yusof et al. [49]	$5x10^5$ cells/ml	50 cells	87%	75%	N/A
Tokar et al. [52]	N/A	50 cells	85-95%	Viable	10 mins
This study	$1x10^4$ - $1x10^5$ cells/ml	10 cells 50 cells 100 cells	82.3 % 90.0 % 96.7 %	87%	10 mins

According to the comparison of accuracy, viability, and duration parameters, the proposed microfluidic device is promising for future improvements on this study.

4.6 Cell Counting Algorithm Results

In order to test the performance of the proposed microfluidic cell counting algorithm, freshly prepared MCF7 cancer cells were used in the test setup mentioned in Chapter 3.4. The experiments were carried out with different inlet sample and microfluidic chips on three different days. Experiments were performed in two replicates each day.

As in the performance experiments, it was desired to collect 10 target cell numbers at the pipette tip. For this purpose, the inlet suspension prepared by serial dilution method at a concentration of $1x10^4$ cells/ml was fed to the chip with negative pressure at a flow rate of 5 µl/min. The region where the outlet port is located, that is, the part where the cells come and rise towards the pipette tip, is accepted as the observation area. After reaching the target cell number, the cells collected at the pipette tip were transferred to the well plate and examined under a fluorescent

microscope to determine the counting accuracy. In order to test the counting algorithm, the video was recorded during the process and counting was performed visually on the video.

Table 4.4 summarizes the data obtained as a result of the 6 experiments. Exp-1 and Exp2; Exp-3 and Exp-4; Exp-5 and Exp-6 were performed on the same days. The same chip and cells were used in experiments performed on the same day. In the Table 4.4, the number of cells collected at the pipette tip examined with the microscope is given together with the counting of cells from the video by eye and with the suggested algorithm. In addition, the errors between counting visually and counting with an algorithm are also given in the table.

Table 4.4 Comparative results of the experiments with different counting methods.

Experiments	***Manual Counting***	***Counting algorithm***	***Error***	***Collected cells***
Exp-1	9	10	1	10
Exp-2	9	9	0	9
Exp-3	12	10	2	12
Exp-4	10	11	1	11
Exp-5	10	9	1	10
Exp-6	10	6	4	10
Total	60	56	9	62

According to the results, while 60 cells were counted visually, 56 cells were counted by the algorithm. The cells collected at the end of each experiment were examined under a microscope and a total of 62 cells were counted. There are 9 total wrong counts between manual counting and the suggested algorithm. The reasons for wrong cell count are as follows: multiple cells coming one after the other, a new cell entering the frame before cell disappears from the frame, cells with very small brightness.

The most important condition for the algorithm to work successfully is the determination of the observation area. Since there is a lot of noise from the environment, the observation area must be chosen carefully to avoid counting errors. Another condition to be considered is the concentration value of the inlet sample. The concentration studied in these experiments is $1x10^4$ cells/ml. However, as the concentration increases, the probability of cells passing through the channel one after another increases. This causes an increase in counting errors.

CHAPTER 5

CONCLUSION AND OUTLOOK

The main objective of this study is to develop a low-cost microfluidic platform for accurate spiking of a low number of cells for analytical performance characterization of rare cell isolation technologies. To achieve this goal, device design, fabrication, and experimental studies were carried out.

The achievements are summarized below:

- A hydrodynamic focusing chip was designed. The focused stream width predicted with the analytic model was verified experimentally.
- Fabrication of the PDMS device was achieved.
- Optimization of the oxygen plasma parameters was accomplished to ensure strong bonding between PDMS and glass. During the study, many experiments were excluded from the analysis due to problems encountered, such as leakage in ports, and low bonding quality. For this reason, it is critical to seal the chip and pay attention to the placement of the ports.
- The experimental setup and the experimental protocol were developed. It was found that the pegylation step in priming the microchannel is critical. In experiments where PEG was not used, problems such as clogging and too much cell adhesion on the channel were observed.
- Flow characterization studies were completed with the pipette tip integrated with FHR, which provides low volume handling on the microfluidic system. As a result of the experiments, response time was longer (>25 seconds) compared to a bare syringe pump. If a lower volume of liquid is desired to be collected, the needle tip can be used instead of the pipette tip. Since the volume of the needle tip is smaller, the stabilization time due to the trapped air will be decreased compared to the pipette tip.

- Flow rate and concentration experiments were completed to determine the operating parameters of the system. Ten cells at a concentration of $1x10^4$ cells/ml and 100 cells at a concentration of $1x10^5$ cells/ml were collected in 10 minutes under 5 µl/min pressure. Cells cannot be counted individually above the flow rate of 10 µl/min and a concentration of $1x10^5$ cells/ml.
- Validation experiments were successfully performed with microbeads and MCF7 cancer cells. The main problem when working with cells is that they are not all the same size or brightness. Cells may be damaged and lose their integrity during sample preparation, dye residues may occur during the staining process, or not all cells may be stained with the same brightness. In such cases, counting cells is very challenging and counting errors increase.
- Cell retrieval in a viable form was confirmed. One of the most important factors that can affect the viability of the cells is the connectors used in the ports. The needle whose tip is blunted with a cutting tool in the laboratory, affects the viability. Therefore blunt-tip needle should be obtained. In addition, connectors should not be inserted all the way through the PDMS ports to the glass slide.
- The image processing algorithm was tested in real-time on three different days. The proposed algorithm is built assuming that the cells pass one by one from the microchannel.

Considering the achievements summarized above, it can be said that the objectives of the thesis were met. However, there are some limitations to be improved. One of the main problems in our study was counting errors due to the long flow response time. This situation has been tried to be overcome with concentration and flow rate adjustments. In addition, as future work, it is suggested to improve the cell counting algorithm for high concentration or flow rate cases. Additionally, if the syringe pump is driven as an image process output, the system becomes a close loop and can be automize in the long term. Regarding the system, a casing or holder can be designed to make the device easy to use and to reduce external noise during image processing.

REFERENCES

[1] E. E. Coyle and M. Oelgemöller, "Micro-photochemistry: photochemistry in microstructured reactors. The new photochemistry of the future?," *Photochem. Photobiol. Sci.*, vol. 7, no. 11, pp. 1313–1322, Oct. 2008, doi: 10.1039/B808778D.

[2] C. D. Chin, V. Linder, and S. K. Sia, "Commercialization of microfluidic point-of-care diagnostic devices," *Lab Chip*, vol. 12, no. 12, pp. 2118–2134, May 2012, doi: 10.1039/C2LC21204H.

[3] C. Yi, C. W. Li, S. Ji, and M. Yang, "Microfluidics technology for manipulation and analysis of biological cells," *Anal. Chim. Acta*, vol. 560, no. 1–2, pp. 1–23, Feb. 2006, doi: 10.1016/J.ACA.2005.12.037.

[4] R. N. Zare and S. Kim, "Microfluidic platforms for single-cell analysis," *Annu. Rev. Biomed. Eng.*, vol. 12, pp. 187–201, Aug. 2010, doi: 10.1146/ANNUREV-BIOENG-070909-105238.

[5] L. Hajba and A. Guttman, "Circulating tumor-cell detection and capture using microfluidic devices," *TrAC Trends Anal. Chem.*, vol. 59, pp. 9–16, Jul. 2014, doi: 10.1016/J.TRAC.2014.02.017.

[6] J. Amontree, K. Chen, J. Varillas, and Z. H. Fan, "Capillary Force Driven Single-Cell Spiking Apparatus for Studying Circulating Tumor Cells," Jan. 2019, doi: 10.1115/IMECE2018-87109.

[7] Y. Zhao, P. G. Schiro, J. S. Kuo, L. Ng, and D. T. Chiu, "Method for the accurate preparation of cell-spiking standards," *Anal. Chem.*, vol. 81, no. 3, pp. 1285–1290, Feb. 2009, doi: 10.1021/AC802250D/ASSET/IMAGES/LARGE/AC-2008-02250D_0001.JPEG.

[8] L. Ding, P. Radfar, M. Rezaei, and M. E. Warkiani, “An easy-to-operate method for single-cell isolation and retrieval using a microfluidic static droplet array,” *Microchim. Acta*, vol. 188, no. 8, pp. 1–11, Aug. 2021, doi: 10.1007/S00604-021-04897-9/FIGURES/4.

[9] T. Hayakawa, T. Fukuhara, K. Ito, and F. Arai, “Single cell separation by using accessible microfluidic chip,” *Proc. IEEE Int. Conf. Micro Electro Mech. Syst.*, pp. 1035–1038, 2014, doi: 10.1109/MEMSYS.2014.6765821.

[10] Y. C. Chen *et al.*, “Selective Photomechanical Detachment and Retrieval of Divided Sister Cells from Enclosed Microfluidics for Downstream Analyses,” *ACS Nano*, vol. 11, no. 5, pp. 4660–4668, May 2017, doi: 10.1021/ACSNANO.7B00413/ASSET/IMAGES/LARGE/NN-2017-004133_0005.JPEG.

[11] K. Tashiro, T. Masuda, and F. Arai, “Single-cell picking by integrated micropipette having sensor for passage detection of cell,” *2014 Int. Symp. Micro-NanoMechatronics Hum. Sci. MHS 2014*, Jan. 2015, doi: 10.1109/MHS.2014.7006139.

[12] RARECYTE, “Single Cell Isolation with the CytePicker Retrieval Module | RareCyte.” .

[13] Apvma, “GUIDELINES FOR THE VALIDATION OF ANALYTICAL METHODS FOR ACTIVE CONSTITUENT, AGRICULTURAL AND VETERINARY CHEMICAL PRODUCTS,” 2004, Accessed: Jul. 30, 2022. [Online]. Available: http://www.apvma.gov.au.

[14] L. Descamps, D. Le Roy, and A. L. Deman, “Microfluidic-Based Technologies for CTC Isolation: A Review of 10 Years of Intense Efforts towards Liquid Biopsy,” *Int. J. Mol. Sci. 2022, Vol. 23, Page 1981*, vol. 23, no. 4, p. 1981, Feb. 2022, doi: 10.3390/IJMS23041981.

[15] A. Gross, J. Schoendube, S. Zimmermann, M. Steeb, R. Zengerle, and P.

Koltay, “Technologies for Single-Cell Isolation,” *Int. J. Mol. Sci.*, vol. 16, no. 8, p. 16897, Jul. 2015, doi: 10.3390/IJMS160816897.

[16] S. Hosic, S. K. Murthy, and A. N. Koppes, “Microfluidic Sample Preparation for Single Cell Analysis,” *Anal. Chem.*, vol. 88, no. 1, pp. 354–380, Jan. 2016, doi: 10.1021/ACS.ANALCHEM.5B04077/ASSET/IMAGES/LARGE/AC-2015-040776_0010.JPEG.

[17] Y. Liu *et al.*, “Advances in Single-Cell Toxicogenomics in Environmental Toxicology,” *Environ. Sci. Technol.*, Jul. 2022, doi: 10.1021/ACS.EST.2C01098.

[18] Y. Reizel *et al.*, “Colon Stem Cell and Crypt Dynamics Exposed by Cell Lineage Reconstruction,” *PLOS Genet.*, vol. 7, no. 7, p. e1002192, Jul. 2011, doi: 10.1371/JOURNAL.PGEN.1002192.

[19] A. Moldavan, “PHOTO-ELECTRIC TECHNIQUE FOR THE COUNTING OF MICROSCOPICAL CELLS,” *Science*, vol. 80, no. 2069, pp. 188–189, 1934, doi: 10.1126/SCIENCE.80.2069.188.

[20] F. T. Gucker, C. T. O’Konski, H. B. Pickard, and J. N. Pitts, “A Photoelectronic Counter for Colloidal Particles,” *J. Am. Chem. Soc.*, vol. 69, no. 10, pp. 2422–2431, 1947, doi: 10.1021/JA01202A053/ASSET/JA01202A053.FP.PNG_V03.

[21] W. H. Coulter, “Means for counting particles suspended in a fluid ,” US2656508A, 1953.

[22] M. J. Fulwyler, “Particle separator ,” US3380584A.

[23] M. J. Fulwyler, “Electronic Separation of Biological Cells by Volume,” *Science (80-.).*, vol. 150, no. 3698, pp. 910–911, Nov. 1965, doi: 10.1126/SCIENCE.150.3698.910.

[24] Dittrich Dr Wolfgang and Goehde Dr Wolfgang, “Automatisches Mess- und Zaehlgeraet fuer die Teilchen einer Dispersion,” DE1815352A1, 1971.

[25] Howard M. Shapiro, *Practical Flow Cytometry*. WILEY.

[26] İ. F. Erturk, “AUTOMATIC CELL COUNTING FROM MICROCHANNEL IMAGES,” 2022.

[27] “How to Count Cells: An Overview of Cell Counting Methods | Logos Biosystems | Advanced Imaging Solutions for Research Excellence,” *Logos Biosystems*, 2018. .

[28] K. Czechowska, D. R. Johnson, and J. R. van der Meer, “Use of flow cytometric methods for single-cell analysis in environmental microbiology,” *Curr. Opin. Microbiol.*, vol. 11, no. 3, pp. 205–212, Jun. 2008, doi: 10.1016/J.MIB.2008.04.006.

[29] J. Wang and Y. Song, “Single cell sequencing: a distinct new field,” *Clin. Transl. Med. 2017 61*, vol. 6, no. 1, pp. 1–11, Feb. 2017, doi: 10.1186/S40169-017-0139-4.

[30] S. Pandey, N. Mehendale, and D. Paul, “Single-Cell Separation,” *Handb. Single Cell Technol.*, pp. 1–28, 2018, doi: 10.1007/978-981-10-4857-9_6-1.

[31] J. Fröhlich and H. König, “New techniques for isolation of single prokaryotic cells,” *FEMS Microbiol. Rev.*, vol. 24, no. 5, pp. 567–572, Dec. 2000, doi: 10.1016/S0168-6445(00)00045-0.

[32] R. Huber, H. Huber, and K. O. Stetter, “Towards the ecology of hyperthermophiles: biotopes, new isolation strategies and novel metabolic properties,” *FEMS Microbiol. Rev.*, vol. 24, no. 5, pp. 615–623, Dec. 2000, doi: 10.1111/J.1574-6976.2000.TB00562.X.

[33] K. Ramser and D. Hanstorp, “Optical manipulation for single-cell studies,” *J. Biophotonics*, vol. 3, no. 4, pp. 187–206, Apr. 2010, doi:

10.1002/JBIO.200910050.

[34] T. Mutanda, D. Ramesh, S. Karthikeyan, S. Kumari, A. Anandraj, and F. Bux, “Bioprospecting for hyper-lipid producing microalgal strains for sustainable biofuel production,” *Bioresour. Technol.*, vol. 102, no. 1, pp. 57–70, Jan. 2011, doi: 10.1016/J.BIORTECH.2010.06.077.

[35] R. Goldman, J. Swedlow, and D. Spector, “Live cell imaging: a laboratory manual,” 2010, Accessed: Aug. 07, 2022. [Online]. Available: http://repository.cshl.edu/29716/.

[36] S. Yilmaz and A. K. Singh, “Single cell genome sequencing,” *Curr. Opin. Biotechnol.*, vol. 23, no. 3, pp. 437–443, Jun. 2012, doi: 10.1016/J.COPBIO.2011.11.018.

[37] P. Hu, W. Zhang, H. Xin, and G. Deng, “Single cell isolation and analysis,” *Front. Cell Dev. Biol.*, vol. 4, no. OCT, p. 116, Oct. 2016, doi: 10.3389/FCELL.2016.00116/BIBTEX.

[38] Molecular Machines & Industries, “Cell Isolation Techniques | Seperation & Transfer.” .

[39] R. Preisig-Müller, M. Mederos y Schnitzler, C. Derst, and J. Daut, “Separation of cardiomyocytes and coronary endothelial cells for cell-specific RT-PCR,” *Am. J. Physiol. - Hear. Circ. Physiol.*, vol. 277, no. 1 46-1, 1999, doi: 10.1152/AJPHEART.1999.277.1.H413/ASSET/IMAGES/LARGE/AHEA40717003W.JPEG.

[40] M. Sun *et al.*, “Precise Aspiration and Positioning Control Based on Dynamic Model Inside and Outside the Micropipette,” *IEEE Trans. Autom. Sci. Eng.*, 2022, doi: 10.1109/TASE.2022.3153901.

[41] G. M. Whitesides, “The origins and the future of microfluidics,” *Nat. 2006 4427101*, vol. 442, no. 7101, pp. 368–373, Jul. 2006, doi:

10.1038/nature05058.

[42] R. C. R. Wootton and A. J. Demello, “Exploiting elephants in the room,” *Nat. 2010 4647290*, vol. 464, no. 7290, pp. 839–840, Apr. 2010, doi: 10.1038/464839a.

[43] T. M. Squires and S. R. Quake, “Microfluidics: Fluid physics at the nanoliter scale,” *Rev. Mod. Phys.*, vol. 77, no. 3, pp. 977–1026, Jul. 2005, doi: 10.1103/REVMODPHYS.77.977/FIGURES/47/MEDIUM.

[44] E. Brouzes *et al.*, “Droplet microfluidic technology for single-cell high-throughput screening,” *Proc. Natl. Acad. Sci. U. S. A.*, vol. 106, no. 34, p. 14195, Aug. 2009, doi: 10.1073/PNAS.0903542106.

[45] D. Di Carlo, L. Y. Wu, and L. P. Lee, “Dynamic single cell culture array,” *Lab Chip*, vol. 6, no. 11, pp. 1445–1449, Oct. 2006, doi: 10.1039/B605937F.

[46] K. Zhang *et al.*, “Hand-Held and Integrated Single-Cell Pipettes,” *J. Am. Chem. Soc.*, vol. 136, no. 31, p. 10858, Aug. 2014, doi: 10.1021/JA5053279.

[47] D. A. Ateya, J. S. Erickson, P. B. Howell, L. R. Hilliard, J. P. Golden, and F. S. Ligler, “The good, the bad, and the tiny: A review of microflow cytometry,” *Anal. Bioanal. Chem.*, vol. 391, no. 5, pp. 1485–1498, Jul. 2008, doi: 10.1007/S00216-007-1827-5/FIGURES/5.

[48] J. Balsam, H. A. Bruck, and A. Rasooly, “Webcam-based flow cytometer using wide-field imaging for low cell number detection at high throughput,” *Analyst*, vol. 139, no. 17, pp. 4322–4329, Jul. 2014, doi: 10.1039/C4AN00669K.

[49] A. Yusof *et al.*, “Inkjet-like printing of single-cells,” *Lab Chip*, vol. 11, no. 14, pp. 2447–2454, Jun. 2011, doi: 10.1039/C1LC20176J.

[50] A. Gross *et al.*, “Single-Cell Printer: Automated, On Demand, and Label Free,” *J. Lab. Autom.*, vol. 18, no. 6, pp. 504–518, Dec. 2013, doi:

10.1177/2211068213497204.

[51] Z. Lu, C. Moraes, G. Ye, C. A. Simmons, and Y. Sun, “Single Cell Deposition and Patterning with a Robotic System,” *PLoS One*, vol. 5, no. 10, p. e13542, 2010, doi: 10.1371/JOURNAL.PONE.0013542.

[52] J. J. Tokar *et al.*, “Pairing Microwell Arrays with an Affordable, Semiautomated Single-Cell Aspirator for the Interrogation of Circulating Tumor Cell Heterogeneity,” *SLAS Technol.*, vol. 25, no. 2, pp. 162–176, Apr. 2020, doi: 10.1177/2472630319898146.

[53] A. Atay *et al.*, “Flow rate-controlled pipetting for microfluidics: second-generation flexible hydraulic reservoir (FHRv2),” *Microfluid. Nanofluidics*, vol. 25, p. 3, 2021, doi: 10.1007/s10404-020-02402-x.

[54] A. Tony, “Design of a microfluidic chip for three dimensional hydrodynamic focusing in cell cytometry applications,” 2011.

[55] M. Serhatlıoğlu, “Development of viscoelastic particle migration for microfluidic flow cytometry applications,” Bilkent University, 2020.

[56] Y. Song, D. Cheng, and L. Zhao, *Microfluidics: Fundamental, Devices and Applications*. Wiley-VCH Verlag GmbH & Co. KGaA, 2018.

[57] K. E. Herold and A. Rasooly, “Lab on a Chip Technology: Fabrication and microfluidics,” p. 425, 2009, Accessed: Jul. 25, 2022. [Online]. Available: https://books.google.com/books?id=Bovn3JO_YLwC.

[58] D. Huber, A. Oskooei, X. Casadevall Solvas, Andrew Demello, and G. V. Kaigala, “Hydrodynamics in Cell Studies,” *Chem. Rev.*, vol. 118, no. 4, pp. 2042–2079, Feb. 2018, doi: 10.1021/ACS.CHEMREV.7B00317/ASSET/IMAGES/LARGE/CR-2017-00317P_0018.JPEG.

[59] D. F. S. Ha, “Development of Microfluidic Chips and a Customised Flow

Control System for use in a Label-Free Cytometer," 2013.

[60] D. F. S. Ha, "Development of Microfluidic Chips and a Customised Flow Control System for use in a Label-Free Cytometer," 2013.

[61] G. Bin Lee, C. C. Chang, S. Bin Huang, and R. J. Yang, "The hydrodynamic focusing effect inside rectangular microchannels," *J. Micromechanics Microengineering*, vol. 16, no. 5, pp. 1024–1032, May 2006, doi: 10.1088/0960-1317/16/5/020.

[62] F. M. White, "Fluid mechanics," p. 862, 2011.

[63] A. Abaza *et al.*, "Hydrodynamic Assists Magnetophoreses Rare Cancer cells Separation in Microchannel Simulation and Experimental Verifications," *IOP Conf. Ser. Mater. Sci. Eng.*, vol. 350, no. 1, p. 012013, May 2018, doi: 10.1088/1757-899X/350/1/012013.

[64] K. W. Oh, K. Lee, B. Ahn, and E. P. Furlani, "Design of pressure-driven microfluidic networks using electric circuit analogy," *Lab Chip*, vol. 12, no. 3, pp. 515–545, Feb. 2012, doi: 10.1039/C2LC20799K.

[65] H. Bruus, *Theoretical microfluidics*. Oxford ; New York: Oxford University Press, 2008.

[66] A. Kalantarifard, E. Alizadeh Haghighi, and C. Elbuken, "Damping hydrodynamic fluctuations in microfluidic systems," *Chem. Eng. Sci.*, vol. 178, pp. 238–247, Mar. 2018, doi: 10.1016/J.CES.2017.12.045.

[67] J. R. Lake, K. C. Heyde, and W. C. Ruder, "Low-cost feedback-controlled syringe pressure pumps for microfluidics applications," *PLoS One*, vol. 12, no. 4, Mar. 2017, doi: 10.1371/JOURNAL.PONE.0175089.

[68] U. Hatipoğlu, B. Cetin, and E. Yildirim, "A novel zero-dead-volume sample loading interface for microfluidic devices: flexible hydraulic reservoir (FHR)," *J. Micromechanics Microengineering*, vol. 28, no. 9, p. 097001,

May 2018, doi: 10.1088/1361-6439/AAC333.

[69] C. E. AKBABA, “Detection of MCF-7 breast cancer cells and monitoring of area, radius, and perimeter developments of them in different days | AVESİS,” Adana Alparslan Türkeş Bilim Ve Teknoloji Üniversitesi, 2021.

[70] A. Ravishankar, S. Anusha, H. K. Akshatha, A. Raj, S. Jahnavi, and J. Madhura, “A survey on noise reduction techniques in medical images,” *Proc. Int. Conf. Electron. Commun. Aerosp. Technol. ICECA 2017*, vol. 2017-January, pp. 385–389, 2017, doi: 10.1109/ICECA.2017.8203711.

[71] C. J. Morales-Perez, J. De Jesus Rangel-Magdaleno, H. Peregrina-Barreto, A. Garcia-Perez, and J. M. Ramirez-Cortes, “Noise Reduction in Electrical Signal Using OMP Algorithm Based on DCT and DSC Dictionaries,” *IEEE Trans. Instrum. Meas.*, vol. 71, 2022, doi: 10.1109/TIM.2021.3135319.

[72] J. Kuruvilla, D. Sukumaran, A. Sankar, and S. P. Joy, “A review on image processing and image segmentation,” *Proc. 2016 Int. Conf. Data Min. Adv. Comput. SAPIENCE 2016*, pp. 198–203, Oct. 2016, doi: 10.1109/SAPIENCE.2016.7684170.

[73] A. A. Theophanous, “A Vehicle Detection, Counting and Tracking system for Traffic Assessment Using Machine Vision and Aerial Video,” 2020.

[74] T. Stiles *et al.*, “Hydrodynamic focusing for vacuum-pumped microfluidics,” *Microfluid. Nanofluidics*, vol. 1, no. 3, pp. 280–283, Jul. 2005, doi: 10.1007/S10404-005-0033-Z.

[75] M. S. Rahim, N. Selamat, J. Yunas, and A. A. Ehsan, “(PDF) Simulation of 3D Hydrodynamic Focusing in Microfluidic Rectangular Shape Microflow Cytometer for Micro Size Cell Application,” 2017, Accessed: Jul. 23, 2022. [Online]. Available: https://www.researchgate.net/publication/318814313_Simulation_of_3D_Hydrodynamic_Focusing_in_Microfluidic_Rectangular_Shape_Microflow_C

ytometer_for_Micro_Size_Cell_Application.

[76] P.-C. Chen, “[PDF] Micromilling Manufacturing for Polymeric Biochips - Free Download PDF,” *Int. Conf. Biosci.*, 2012, Accessed: Jun. 01, 2022. [Online]. Available: https://nanopdf.com/download/micromilling-manufacturing-for-polymeric-biochips_pdf.

[77] A. S. Kumar, S. Deb, and S. Paul, “Ultrasonic-assisted abrasive micro-deburring of micromachined metallic alloys,” *J. Manuf. Process.*, vol. 66, pp. 595–607, Jun. 2021, doi: 10.1016/J.JMAPRO.2021.04.019.

[78] S. L. Peterson, A. McDonald, P. L. Gourley, and D. Y. Sasaki, “Poly(dimethylsiloxane) thin films as biocompatible coatings for microfluidic devices: cell culture and flow studies with glial cells,” *J. Biomed. Mater. Res. A*, vol. 72, no. 1, pp. 10–18, Jan. 2005, doi: 10.1002/JBM.A.30166.

[79] “Fluoresbrite® YG Microspheres 20.0µm | Polysciences, Inc.” https://www.polysciences.com/german/fluoresbrite-yg-microspheres-200m-43713 (accessed Feb. 13, 2022).

[80] G. Özkayar *et al.*, “A Novel Microfluidic Method Utilizing a Hydrofoil Structure to Improve Circulating Tumor Cell Enrichment: Design and Analytical Validation,” *Micromachines 2020, Vol. 11, Page 981*, vol. 11, no. 11, p. 981, Oct. 2020, doi: 10.3390/MI11110981.

[81] H. Hardelauf *et al.*, “High fidelity neuronal networks formed by plasma masking with a bilayer membrane: analysis of neurodegenerative and neuroprotective processes,” *Lab Chip*, vol. 11, no. 16, pp. 2763–2771, Aug. 2011, doi: 10.1039/C1LC20257J.

[82] Y. Demircan Yalçın, “A Lab-on-a-chip system integrating dielectrophoretic detection and impedance counting units for chemotherapy guidance in leukemia,” 2018, Accessed: Aug. 24, 2022. [Online]. Available:

https://open.metu.edu.tr/handle/11511/27297.

[83] L. Campo-Deaño, “Fluid-Flow Characterization in Microfluidics,” *Complex Fluid-Flows Microfluid.*, pp. 53–71, May 2018, doi: 10.1007/978-3-319-59593-1_3.

[84] “Manual Tracking.” https://imagej.nih.gov/ij/plugins/track/track.html (accessed Jun. 01, 2022).

[85] J. M. Martel and M. Toner, “Inertial focusing in microfluidics,” *Annual Review of Biomedical Engineering*, vol. 16. Annual Reviews Inc., pp. 371–396, May 29, 2014, doi: 10.1146/annurev-bioeng-121813-120704.

[86] “TC20 Automated Cell Counter | Bio-Rad.” https://www.bio-rad.com/en-tr/product/tc20-automated-cell-counter?ID=M7FBG34VY (accessed Jun. 22, 2022).

[87] I. J. Fang and B. G. Trewyn, “Application of Mesoporous Silica Nanoparticles in Intracellular Delivery of Molecules and Proteins,” *Methods Enzymol.*, vol. 508, pp. 41–59, Jan. 2012, doi: 10.1016/B978-0-12-391860-4.00003-3.

[88] G. Xie and W. Lu, “Image Edge Detection Based On Opencv,” *undefined*, vol. 1, no. 2, pp. 104–106, 2013, doi: 10.12720/IJEEE.1.2.104-106.

[89] V. Y. Borole, S. Nimbhore, and D. S. S. Kawthekar, “Image Processing Techniques for Brain Tumor Detection : A Review,” 2015.

[90] D. Li, B. Liang, and W. Zhang, “Real-time moving vehicle detection, tracking, and counting system implemented with OpenCV,” *ICIST 2014 - Proc. 2014 4th IEEE Int. Conf. Inf. Sci. Technol.*, pp. 631–634, Oct. 2014, doi: 10.1109/ICIST.2014.6920557.

[91] W. Zeng, S. Li, and Z. Wang, “Characterization of syringe-pump-driven versus pressure-driven microfluidic flows,” *Proc. 2015 Int. Conf. Fluid*

Power Mechatronics, FPM 2015, pp. 711–715, Nov. 2015, doi: 10.1109/FPM.2015.7337207.

[92] V. K. Jagannadh, J. V. Adhikari, and S. S. Gorthi, "Automated cell viability assessment using a microfluidics based portable imaging flow analyzer," *Biomicrofluidics*, vol. 9, no. 2, p. 024123, Apr. 2015, doi: 10.1063/1.4919402.

[93] Y. J. Heo, D. Lee, J. Kang, K. Lee, and W. K. Chung, "Real-time Image Processing for Microscopy-based Label-free Imaging Flow Cytometry in a Microfluidic Chip," *Sci. Reports 2017 71*, vol. 7, no. 1, pp. 1–9, Sep. 2017, doi: 10.1038/s41598-017-11534-0.

APPENDICES

A. MATLAB Simulink Model

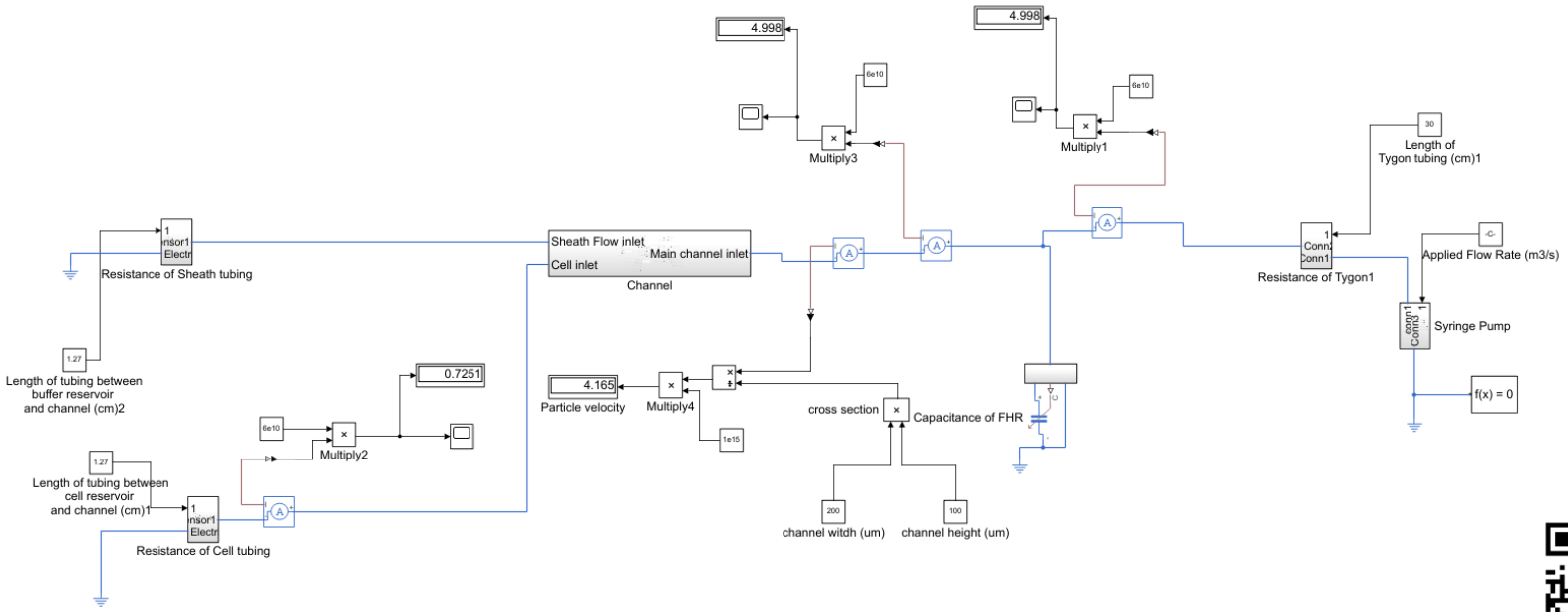

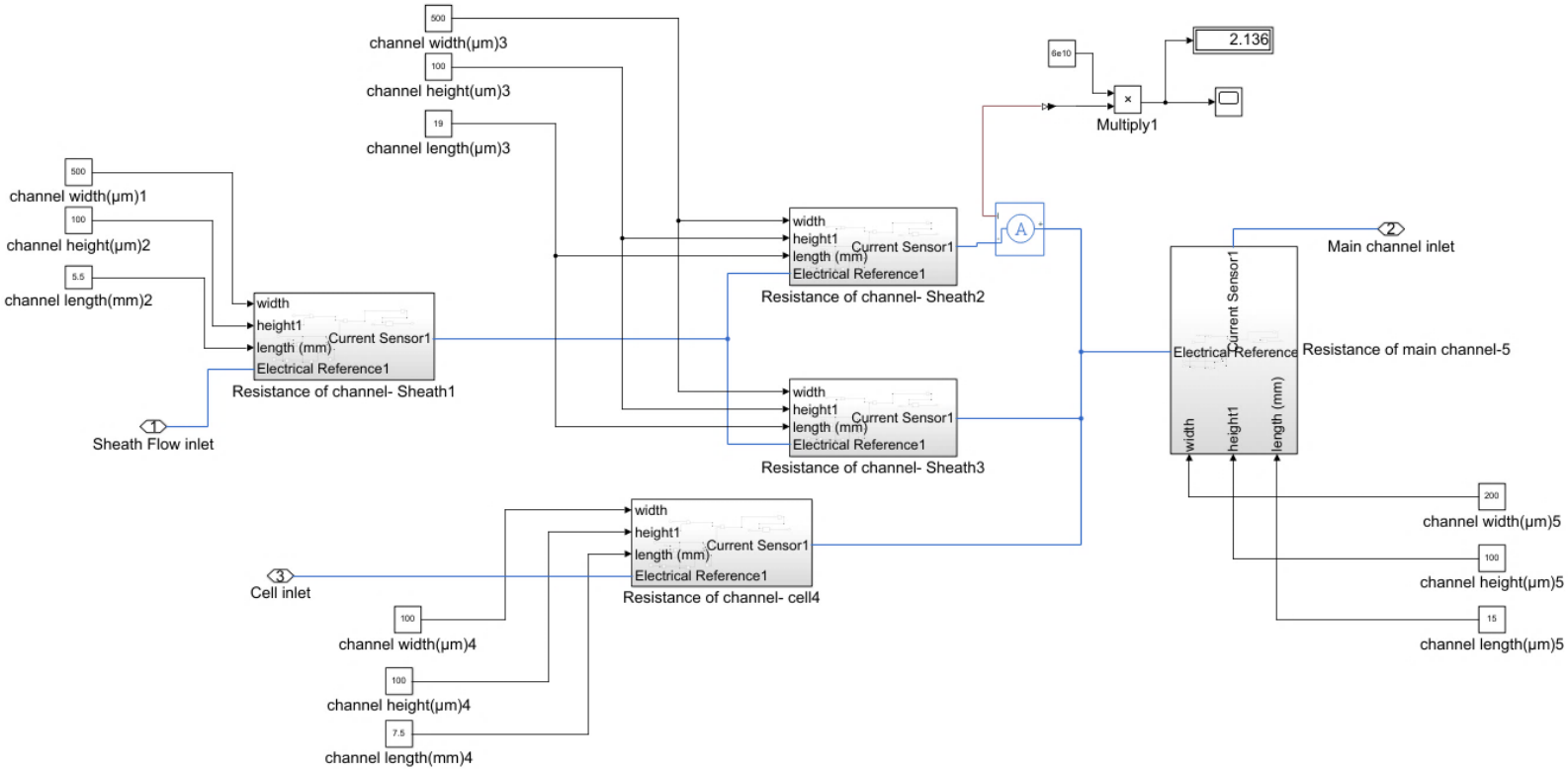
500
channel width(μm)3
100
channel height(um)3
19
channel length(μm)3
500
channel width(μm)1
100
channel height(μm)2
5.5
channel length(mm)2
width
height1
length (mm)
Current Sensor1
Electrical Reference1
Resistance of channel- Sheath1
1
Sheath Flow inlet
width
height1
length (mm)
Current Sensor1
Electrical Reference1
Resistance of channel- Sheath2
width
height1
length (mm)
Current Sensor1
Electrical Reference1
Resistance of channel- Sheath3
6e10
Multiply1
2.136
2
Main channel inlet
Current Sensor1
Electrical Reference
Resistance of main channel-5
width
height1
length (mm)
200
channel width(μm)5
100
channel height(μm)5
15
channel length(μm)5
width
height1
length (mm)
Current Sensor1
Electrical Reference1
Resistance of channel- cell4
3
Cell inlet
100
channel width(μm)4
100
channel height(μm)4
7.5
channel length(mm)4